



Publication Year	2006
Acceptance in OA @INAF	2024-01-29T14:49:53Z
Title	Planetary nebulae as tracers of galaxy stellar populations
Authors	BUZZONI, Alberto; Arnaboldi, Magda; Corradi, Romano L. M.
DOI	10.1111/j.1365-2966.2006.10163.x
Handle	http://hdl.handle.net/20.500.12386/34642
Journal	MONTHLY NOTICES OF THE ROYAL ASTRONOMICAL SOCIETY
Number	368

Planetary nebulae as tracers of galaxy stellar populations

Alberto Buzzoni,^{1★} Magda Arnaboldi^{2,3★} and Romano L. M. Corradi^{4,5★}

¹INAF – Osservatorio Astronomico di Bologna, Via Ranzani 1, 40127 Bologna, Italy

²ESO – Karl-Schwarzschild-Str. 2, 85748 Garching bei München, Germany

³INAF – Osservatorio Astronomico di Torino, Via Osservatorio 20, 10025 Pino Torinese (To), Italy

⁴ING – Isaac Newton Group of Telescopes, A.P. 321, 38700 Santa Cruz de La Palma, Spain

⁵IAC – Instituto de Astrofísica de Canarias, Via Láctea s/n, 38200 La Laguna, Tenerife, Spain

Accepted 2006 February 7. Received 2006 January 20; in original form 2005 November 11

ABSTRACT

We address the general problem of the luminosity-specific planetary nebula (PN) number, better known as the ‘ α ’ ratio, given by $\alpha = N_{\text{PN}}/L_{\text{gal}}$, and its relationship with the age and metallicity of the parent stellar population. Our analysis relies on population synthesis models that account for simple stellar populations (SSPs), and more elaborate galaxy models covering the full star formation range of the different Hubble morphological types. This theoretical framework is compared with the updated census of the PN population in Local Group (LG) galaxies and external ellipticals in the Leo group, and the Virgo and Fornax clusters.

The main conclusions of our study can be summarized as follows.

(i) According to the post-asymptotic giant branch (AGB) stellar core mass, PN lifetime in a SSP is constrained by three relevant regimes, driven by the nuclear ($M_{\text{core}} \gtrsim 0.57 M_{\odot}$), dynamical ($0.57 M_{\odot} \gtrsim M_{\text{core}} \gtrsim 0.55 M_{\odot}$) and transition ($0.55 M_{\odot} \gtrsim M_{\text{core}} \gtrsim 0.52 M_{\odot}$) time-scales. The lower limit for M_{core} also sets the minimum mass for stars to reach the AGB thermal-pulsing phase and experience the PN event.

(ii) Mass loss is the crucial mechanism to constrain the value of α , through the definition of the initial-to-final mass relation (IFMR). The Reimers mass-loss parametrization, calibrated on Pop II stars of Galactic globular clusters, poorly reproduces the observed value of α in late-type galaxies, while a better fit is obtained using the empirical IFMR derived from white dwarf observations in the Galaxy open clusters.

(iii) The inferred PN lifetime for LG spirals and irregulars exceeds 10 000 yr, which suggests that $M_{\text{core}} \lesssim 0.65 M_{\odot}$ cores dominate, throughout.

(iv) The relative PN deficiency in elliptical galaxies, and the observed trend of α with galaxy optical colours, support the presence of a prevailing fraction of low-mass cores ($M_{\text{core}} \lesssim 0.55 M_{\odot}$) in the PN distribution and a reduced visibility time-scale for the nebulae as a consequence of the increased AGB transition time. The stellar component with $M_{\text{core}} \lesssim 0.52 M_{\odot}$, which overrides the PN phase, could provide an enhanced contribution to hotter HB and post-HB evolution, as directly observed in M 32 and the bulge of M 31. This implies that the most UV-enhanced ellipticals should also display the lowest values of α , as confirmed by the Virgo cluster early-type galaxy population.

(v) Any blue-straggler population, invoked as progenitor of the $M_{\text{core}} \gtrsim 0.7 M_{\odot}$ PNe in order to preserve the constancy of the bright luminosity-function cut-off magnitude in ellipticals, must be confined to a small fraction (a few per cent at most) of the whole galaxy PN population.

Key words: ISM: lines and bands – Galaxy: fundamental parameters – galaxies: evolution – galaxies: spiral – galaxies: stellar content.

*E-mail: buzzoni@bo.astro.it (AB); marnabol@eso.org (MA); rcorradi@

ing.iac.es (RLMC)

© 2006 The Authors. Journal compilation © 2006 RAS

1 INTRODUCTION

Diffuse intracluster luminosity (Uson, Boughn & Kuhn 1991) and other faint surface-brightness features detected at large distances from the centre of isolated and cluster galaxies (Hui et al. 1993; Mihos et al. 2005) may provide a valuable record of the mechanisms that led to the assembly and formation of the cosmic structures at the different hierarchical scales.

Stellar streams, like the case of Sgr and CMa in the Milky Way (e.g. Martin et al. 2004), and ‘runaway’ halo stars (Blaauw 1961; Keenan & Dufton 1983; Allen & Kinman 2004) are, in this sense, excellent examples of the effect of galaxy tidal interactions and dynamical relaxation processes that spread stars well outside the bright body of their parent systems. Furthermore, the evidence of quiescent on-going star formation in low-density environments, such as dwarf or very low surface-brightness galaxies (Hunter & Gallagher 1985; Caldwell 1995; Cellone & Buzzoni 2005), indicates that the transition between coherent stellar systems and diffuse background might be not so sharp.

In this framework, the study of planetary nebulae (PNe) is of special interest as these objects are efficient tracers of their underlying parent stellar population even in those regions where the stellar plot is too faint to be detected against the night-sky brightness (Arnaboldi et al. 2003). Relying on standard narrow-band imagery, PNe have been confidently detected out to 70 kpc from the centre of Cen A (Hui et al. 1993) and other bright galaxies in the Virgo and Fornax clusters, about 15 Mpc away (Arnaboldi et al. 2003, 2004; Feldmeier et al. 2003, 2004; Peng, Ford & Freeman 2004; Aguerri et al. 2005). On the other hand, optimized multislit imaging recently pushed this distance limit even farther, reaching the Coma cluster PNe, at about 100-Mpc distance (Gerhard et al. 2005).

One open question in this approach is the link between the size of the PN component and the sampled (bolometric) luminosity of its parent stellar population. This ratio, often referred to in the literature as the ‘luminosity-specific PN number density’ or, shortly, the ‘ α ratio’ (Jacoby 1980), provides the amount of light associated to any observed PN sample, and it is the first assumption when using PNe as tracers of the spatial distribution and motions of the parent stars. Observationally, there is strong evidence for α to correlate with galaxy colour, the reddest ellipticals being a factor 5–7 poorer in PNe per unit galaxy luminosity than spirals (Peimbert 1990; Hui et al. 1993). This trend is at odds with a nearly ‘universal’ PN luminosity function (PNLF), as observed for galaxies along the whole Hubble morphological sequence (Ciardullo et al. 2002a).

Population synthesis models offer a useful reference tool, in this regard, as they allow us to probe the theoretical relationship of α with the different distinctive parameters of a stellar population, thus overcoming most of the observational uncertainties related to systematic bias, incomplete sampling etc. In addition, a theoretical assessment of the α ratio does not require, in principle, any exact knowledge of the PNLF, still largely uncertain at its faint magnitudes (Jacoby & De Marco 2002; Jacoby 2006).

In this paper, we want to study the luminosity-specific PN number density from a more general approach based on a new set of stellar population models. Our calculations rely on the (Buzzoni 1989, hereafter B89) and Buzzoni (1995) synthesis code, including the recent extension to template galaxy models of composite star formation (Buzzoni 2002, 2005). Our predictions for the α ratio will also be compared with the observed PN population of Local Group (LG) galaxies to validate our adopted scenario for post-asymptotic giant branch (PAGB) evolution. We will also address the puzzling problem of the poorer PN population in elliptical galaxies (Hui et al.

1993): this very interesting feature might be the signature of a phase transition related to horizontal branch (HB) evolution, with important consequences on the expected ultraviolet (UV) evolution of galaxies and other stellar systems in metal-rich environments.

Our paper will be organized as follows: in Section 2 we shall present the simple stellar population (SSP) theory, and discuss the relevant parameters that constrain α . Section 3 is devoted to the expected theoretical values of the α parameter for galaxies of different morphological type. In Section 4, we compare the theoretical results with observations of the PN population in LG and external galaxies in the Leo group, the Virgo and Fornax clusters. In Section 5, we study the correlation between α and other spectrophotometric indices for early-type galaxy diagnostic, like the Lick Mg_2 index and the (1550 – V) UV colour. Finally, in Section 6, we summarize the constraints obtained for the PAGB evolution and the relevant time-scale for PN evolution.

2 SIMPLE STELLAR POPULATION THEORY

The SSP theory developed by (Renzini & Buzzoni 1986, hereafter RB86) and B89 allows us to compute the value of α for a coeval and chemically homogeneous stellar aggregate. Assuming a standard power-law initial mass function (IMF) such as $N_*(M_*) \propto M_*^{-s} dM_*$, the expected number of stars that populate the ‘ j ’th post-main sequence (PMS) phase, of duration τ_j , can be written as

$$N_j = AM_{\text{TO}}^{-s} |\dot{M}_{\text{TO}}| \tau_j, \quad (1)$$

where \dot{M}_{TO} is the time derivative of the MS turn off (TO) mass. The scaling factor A in equation (1) accounts for the total mass of the SSP (cf. B89), and relates to the total luminosity of the stellar population, so that $N_j \propto L_{\text{tot}} \tau_j$.

When this approach is applied to the PN phase, it becomes

$$N_{\text{PN}} = \mathcal{B} L_{\text{tot}} \tau_{\text{PN}}, \quad (2)$$

where $\mathcal{B} = AM_{\text{TO}}^{-s} |\dot{M}_{\text{TO}}| / L_{\text{tot}}$ is the so-called ‘specific evolutionary flux’ (see RB86 and B89), and τ_{PN} is the PN *visibility* lifetime, i.e. the time for the nebula to be detectable in [O III] and/or H α surveys. The value of the ‘luminosity-specific PN number’ α simply derives from equation (2) as

$$\alpha = \frac{N_{\text{PN}}}{L_{\text{tot}}} = \mathcal{B} \tau_{\text{PN}}. \quad (3)$$

Therefore, two parameters, that is \mathcal{B} and τ_{PN} , set the value of the luminosity-specific PN number for a given SSP.

2.1 The ‘specific evolutionary flux’ \mathcal{B}

This parameter links the PN rate to the evolutionary properties of the parent stellar population. It contains, in fact, (i) the physical ‘clock’ of the population (as both M_{TO} and \dot{M}_{TO} depend on time), and (ii) the IMF dependence, because the ratio A/L_{tot} closely scales with the SSP M/L ratio, thus responding to the mass distribution of the composing stars.

Following Buzzoni (1998), we can further arrange our definition of \mathcal{B} and write

$$\mathcal{B} = \frac{AM_{\text{TO}}^{-s} |\dot{M}_{\text{TO}}|}{L_{\text{tot}}} = \frac{\mathcal{L}}{\text{PMS fuel}}. \quad (4)$$

The right-hand side of equation (4) derives from the RB86 ‘Fuel consumption theorem’ and identifies the PMS contribution to the total SSP luminosity ($\mathcal{L} = L_{\text{PMS}}/L_{\text{tot}}$), as well as the *absolute* nuclear fuel spent during PMS evolution by stars with $M_* = M_{\text{TO}}$.

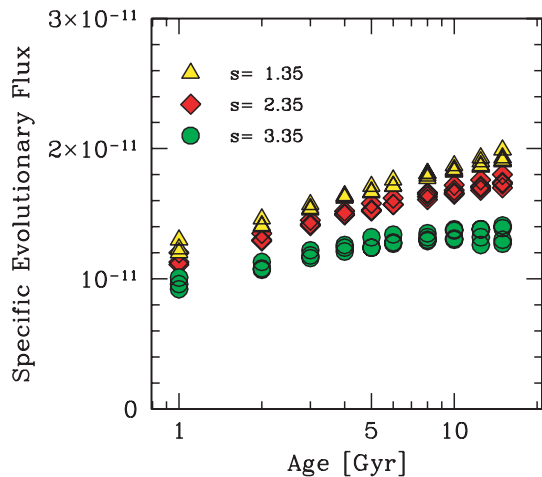


Figure 1. Specific evolutionary flux B , from equation (4), for B89 SSP models. Different metallicity sets (between $Z \sim 1/20$ and $2Z_{\odot}$) are over-plotted. In addition to the Salpeter case ($s = 2.35$), other IMF power-law coefficients are explored, as labelled on the plot. The value of B is given in units of $L^{-1}_{\odot} \text{yr}^{-1}$.

As pointed out by RB86, B does not change much with metallicity or IMF slope; this is shown in Fig. 1, where we display the specific evolutionary flux, according to B89 SSP models, for different IMF slopes and metallicity. One can see that models with $Z = 1/20$ to $2Z_{\odot}$ and IMF slopes from 1.35 to 3.35 changes B by only a factor of 2, at most, over a wide range of SSP age, from 1 to 15 Gyr.

The dependence of α on the IMF slope is through the change in \mathcal{L} , i.e. the relative PMS luminosity contribution in equation (4). In general, a giant-dominated SSP will display a larger value of α because giant stars become more important in a ‘flatter’ IMF and \mathcal{L} tends to increase, compared to the Salpeter $s = 2.35$ case. On the other hand, a younger age acts in the sense of decreasing the PN rate per unit SSP luminosity, because the MS luminosity contribution increases, the absolute amount of ‘fuel’ burnt by PMS stars increases (cf. e.g. fig. 3 in RB86), and \mathcal{L} decreases.

2.2 The PN lifetime τ_{PN}

This quantity depends both on the chemical and dynamical properties of the ejected material, giving rise to the nebular envelope, and on the stellar core-mass evolution, which is responsible for the ‘firing up’ of the nebular gas.

The first self-consistent theoretical model of PN core evolution is due to Paczyński (1971), then followed by contributions from Schönberner (1981, 1983), Górny, Tylenda & Szczerba (1994), Vassiliadis & Wood (1994), Stanghellini (1995), Stanghellini & Renzini (2000) and more recently by Marigo et al. (2001) and Perinotto et al. (2004a). Theory predicts that the PN properties strongly depend on the core-mass distribution of PAGB remnants, the latter being the result of the initial-to-final mass relation (IFMR), as modulated by metallicity and mass loss. The so-called ‘transition time’ for PAGB stars to reach the high-temperature region ($T_{\text{eff}} \gtrsim 30000 \text{ K}$), after the nebula ejection, may also play a role on the emission properties and the time-scale of the PN event.

A simple estimate of PN core lifetime can be derived from the energetic budget available to PAGB stars. This is computed in Fig. 2, based on a model collection from Paczyński (1971), Schönberner (1981, 1983) and Vassiliadis & Wood (1994). Indeed, one sees that Paczyński (1971) original results consistently meet the more recent

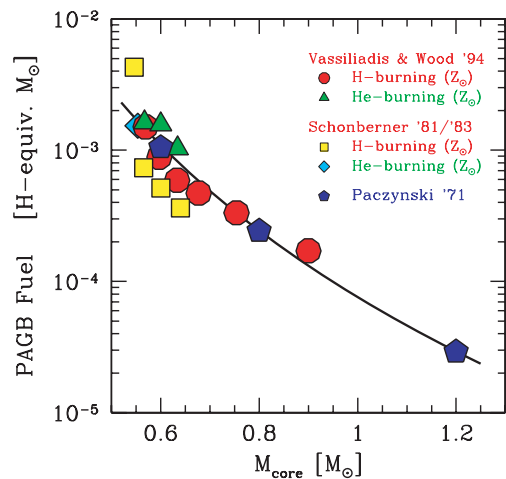


Figure 2. Theoretical fuel consumption for stars along the PAGB evolution according to different model sets: (Paczyński 1971, pentagon markers), (Schönberner 1981, 1983, squares and rhombs), (Vassiliadis & Wood 1994, dots and triangles). The different markers for the same model source refer to the prevailing case of a H or He thermal pulse terminating the AGB evolution, as labelled. Fuel is expressed in Hydrogen-equivalent solar mass, i.e. 1 g of H-equivalent mass = $6 \cdot 10^{18} \text{ erg}$ (cf. RB86), and a solar metallicity is assumed in the models. A smooth analytical relation matching the data, according to equation (5) is plotted as a solid curve.

and sophisticated stellar tracks, like those of Vassiliadis & Wood (1994), that account for stellar envelope ejection either in the case of a He or H thermal pulse at the tip of asymptotic giant branch (AGB) evolution.

From B89, an analytical function that reproduces the PAGB fuel consumed as a function of the core mass for the different theoretical data sets of Fig. 2 is

$$\text{PAGB fuel} = (M_{\text{core}}/0.163)^{-5.22} [H M_{\odot}], \quad (5)$$

where M_{core} is in solar unit and fuel in Hydrogen-equivalent solar mass (cf. Fig. 2 for details). The PAGB stellar lifetime can be defined as

$$\tau_{\text{PAGB}} \simeq (\text{PAGB fuel}/\ell_{\text{PAGB}}), \quad (6)$$

being ℓ_{PAGB} the luminosity of the stellar core at the onset of the nebula ejection (see e.g. Paczyński 1971). In general, τ_{PAGB} is shorter than the estimated dynamical time-scale for the nebula evaporation, which is about $\tau_{\text{dyn}} \simeq 30000 \text{ yr}$ (cf. Schönberner 1983; Phillips 1989), and this implies that for SSPs of young and intermediate age $\tau_{\text{PN}} \simeq \tau_{\text{PAGB}}$.

On the other hand, when the SSP age increases, this assumption may no longer hold, and at some point, when PAGB stellar core mass decreases and $M_{\text{core}} \lesssim 0.57 M_{\odot}$, τ_{PAGB} starts to exceed τ_{dyn} . Henceforth, the PN evolution is driven by the dynamical time-scale, reduced by the transition time.

2.3 PAGB core mass and PN evolution

As M_{core} constrains both the fuel and PAGB luminosity, from which τ_{PAGB} derives,¹ it is clear that mass-loss mechanisms, at work along the giant-branch evolution, set the leading parameters for PN evolution. In this sense, it is of paramount importance to establish a

¹ In force of equation (5), and also considering that $\ell_{\text{PAGB}} \propto M_{\text{core}}$ in equation (6) (Paczyński 1971), we have that $\tau_{\text{PAGB}} \propto M_{\text{core}}^{-6.22}$.

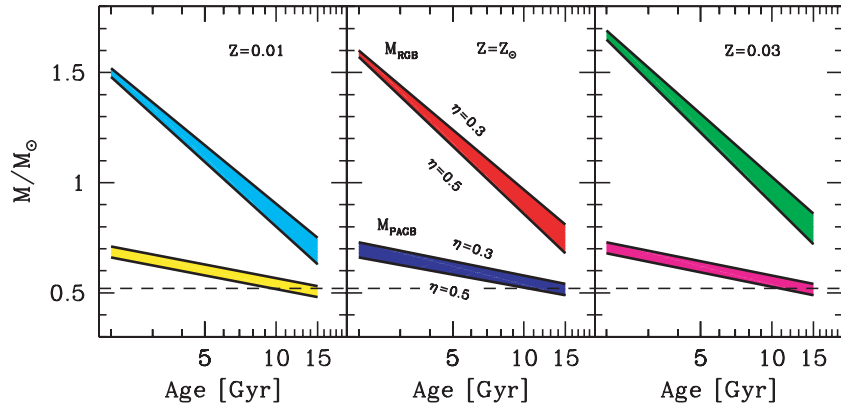


Figure 3. Time evolution of the stellar mass at some tipping points across the H–R diagram for SSPs of different metallicity Z , about the solar value, as labelled in each panel. Upper strips in each panel are the theoretical loci for stellar mass at the tip of the RGB evolution (M_{RGB}) according to a Reimers mass-loss parameter in the range $0.3 \leq \eta \leq 0.5$, as labelled in the middle panel, for general reference. Lower strips mark the locus for stellar mass at the onset of PAGB evolution (M_{PAGB}), again for the same reported range of the mass-loss parameter η . The minimum mass for stars to reach the AGB thermal pulsing phase (and eventually produce a PN) is marked by the dashed line, according to Dorman et al. (1993) and Blöcker (1995).

suitable relationship between the initial (i.e. $M_i \equiv M_{\text{TO}}$) and final ($M_f \equiv M_{\text{PAGB}}$) mass of stars along the whole SSP evolution.

A firm settlement of the IFMR is a long-standing problem, that has been addressed both theoretically (Iben & Renzini 1983, hereafter IR83; Dominguez et al. 1999; Girardi et al. 2000) and observationally (Weidemann & Koester 1983; Weidemann 1987, 2000, hereafter W00; Claver et al. 2001; Kalirai et al. 2005).

2.3.1 Mass loss and M_{core} : the theoretical approach

A direct evaluation of the mass loss, according to the Reimers (1975) theoretical parameterization, is shown in Fig. 3. In this figure, we plot the expected value of stellar masses at some tipping points of SSP evolution, for three relevant values of metallicity around the solar value. In particular, M_{RGB} is the mass of stars at the end of red giant branch (RGB) evolution, which occurs after the first important mass-loss episode experienced by stars at the low-gravity low-temperature regime; M_{PAGB} is then the mass of the stars leaving the AGB, after the second stronger mass-loss episode. The trend of both quantities is tracked versus SSP age, for a range of the Reimers mass-loss parameter, η , between 0.3 and 0.5.²

Along the SSP evolution shown in Fig. 3, a substantial fraction (up to 50 per cent) of the stellar mass is lost during the AGB phase (cf. the difference $\Delta M_* = M_{\text{RGB}} - M_{\text{PAGB}}$ on the plots); furthermore, with increasing age, the core mass of PAGB stars approaches (or even crosses) the limit of $M_{\text{PAGB}} \simeq 0.52 M_{\odot}$, which is the minimum mass required by models for stars to experience the so-called AGB ‘thermal-pulsing’ phase (Dorman, Rood & O’Connell 1993; Blöcker 1995). During this phase, stars venture in the region of Mira variables and end their AGB evolution with a quick envelope ejection, likely driven by dynamical instability (the so-called ‘superwind phase’ of Renzini 1981), and the subsequent PN stage (see Paczyński 1970, and IR83, for an exhaustive discussion of the process and its variants). We shall discuss the implication of an inhibited AGB phase on PN evolution in what follows.

² A value of $\eta \simeq 0.4 \pm 0.1$ is typically required in order to reproduce the observed colour–magnitude (c–m) diagram of old Galactic globular clusters (Fusi Pecci & Renzini 1976).

2.3.2 Mass loss and M_{core} : the empirical approach

The IFMR can be derived empirically from the mass estimate of observed white dwarfs in nearby open clusters (like Hyades or Praesepe), coupled with the value of M_{TO} and cluster age, as obtained from isochrone fit of the cluster c–m diagram.

Quoting W00, there is evidence that observed white dwarf masses, for low- and intermediate-mass stars, ‘coincide almost exactly with the new theoretical predictions of the core masses at the beginning of the thermal pulsing AGB’ (M_{TP}). In addition, ‘it is presumed and supported weakly by the empirical data that this closeness of the final mass to the first-thermal pulse core mass relation continues also to higher initial masses’, possibly up to the limit of SN onset (roughly placed about $7 M_{\odot}$).

The first claim of this analysis is confirmed by Fig. 4, where we compare the W00 IFMR and the theoretical estimates of M_{TP} from

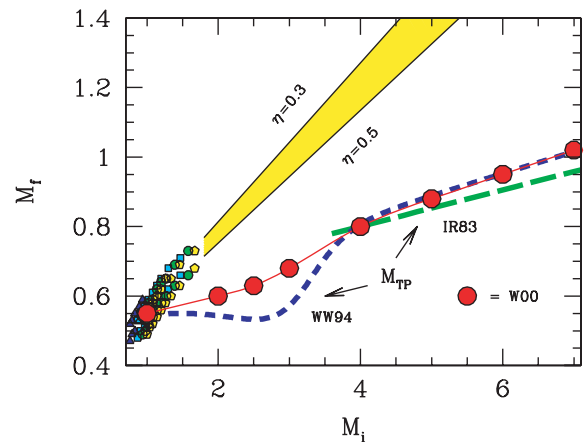


Figure 4. The IFMR according to different calibrations. The solid strip is the theoretical relation of IR83 for a standard mass-loss parameter η in the range between 0.3 and 0.5, as labelled on the plot. Small dots report the individual values as from the B89 SSP models of Table 1 and the same Reimers parameters. Short- and long-dashed curves are the theoretical loci for stars to set on the AGB thermal pulsing phase (M_{TP}), according to IR83 and Wagenhuber & Weiss (1994) (WW94). Finally, big dots and solid curve report the W00 empirical relation based on the mass estimate of white dwarfs in Galactic open cluster.

an updated set of stellar tracks for Pop I stars by Wagenhuber & Weiss (1994) and from the original analytical relation by IR83 for intermediate-mass stars, namely

$$M_{\text{TP}} = 0.59 + 0.0526 M_i. \quad (7)$$

It is also clear from Fig. 4 that, for a standard range of Reimers mass-loss parameters fitted to Galactic globular clusters, the IR83 theoretical IFMR overestimates the value of M_i for young ($t \lesssim 2$ Gyr) SSPs, requiring a value of $\eta \gg 1$ to match the W00 empirical relation.

Given the discrepancy between the predicted M_{core} based on the standard mass-loss theory *à la* Reimers (1975) and the observations by W00, we compute the τ_{PAGB} values according to (a) a theoretical IFMR according to B89 SSP models with $\eta = 0.3$, extended to younger ages through the IR83 relation

$$M_{\text{core}} = 0.53 \eta^{-0.082} + 0.15 \eta^{-0.35} (M_{\text{TO}} - 1), \quad (8)$$

and (b) the W00 empirical IFMR, as displayed in Fig. 4.

2.3.3 A critical core mass range: $0.52 M_{\odot} \leq M_{\text{core}} \leq 0.55 M_{\odot}$

When the core nuclear lifetime ceases to be the driving parameter for PN visibility (that is for $M_{\text{core}} \lesssim 0.57 M_{\odot}$), we have that $\tau_{\text{PN}} \simeq (\tau_{\text{dyn}} - \tau_{\text{tt}})$, where τ_{tt} is the transition time of the stellar core to become hot enough such as to ‘fire up’ the nebula. Models show that, for $M_{\text{core}} \lesssim 0.55 M_{\odot}$, τ_{tt} abruptly increases from its typical value range of 200–2000 yr up to exceeding τ_{dyn} (Schönberner 1983; Vassiliadis & Wood 1994). In this case, by the time the stellar core is there ready to heat, the gaseous shell has already evaporated, thus preventing the nebula ignition. The dynamical time-scale itself is slightly influenced by mass loss as a slower envelope expansion, driven by radiation pressure, is expected if η increases such as to terminate AGB evolution at lower luminosity (Vassiliadis & Wood 1994; Marigo et al. 2001; Villaver, Manchado & García-Segura 2002).

In general, this scenario leads to conclude that in old SSPs PN visibility might be greatly reduced or even fully inhibited as a consequence of a delayed hot-PAGB evolution of the stellar core (Stanghellini & Renzini 2000).

In addition, one has also to account for a further critical threshold in the evolutionary framework when stars escape the AGB thermal-pulsing phase, for $M_{\text{core}} \lesssim 0.52 M_{\odot}$. The lack of a full AGB development leads to a range of post-HB evolutionary paths,³ as discussed in detail by Greggio & Renzini (1990). One relevant case, in this regard, is that of ‘AGB-manqué’ stars, that directly set on the high-temperature white dwarf cooling sequence after leaving the HB, thus missing, partially or *in toto*, the AGB phase. First important hints of this non-standard evolutionary framework can be found in the original work of Gingold (1974), and a number of later contributions tried to better assess the critical parameters (mass loss *in primis*) involved in the process (Castellani, Limongi & Tornambé 1992, 1995; Dorman et al. 1993; D’Cruz et al. 1996; Yi, Demarque & Oemler 1998; Castellani et al. 2006).

The impact of this composite scenario on the PN formation mechanisms is probably still to be fully understood; it seems clear, however, that a full completion of AGB evolution, up to the thermal-pulsing luminosity range, is the most viable step to culminate with

the nebula event (see also Kwok 1994, for a more elaborated discussion in this regard).

2.4 The luminosity-specific PN number in simple stellar populations

According to the previous discussion, the luminosity-specific PN number in a SSP can eventually be written as

$$\alpha = \begin{cases} \mathcal{B} \min[\tau_{\text{PAGB}}, (\tau_{\text{dyn}} - \tau_{\text{tt}})] & \text{if } \tau_{\text{tt}} \leq \tau_{\text{dyn}}, \\ 0 & \text{otherwise.} \end{cases} \quad (9)$$

In general, τ_{dyn} sets a safe upper limit to the α value. For a Salpeter IMF, and from the data of Fig. 1, we derive

$$\alpha_{\text{max}} \simeq 1.8 \times 10^{-11} \times 30\,000 = \frac{1 \text{ PN}}{1.85 \times 10^6 L_{\odot}}. \quad (10)$$

This value is virtually independent from metallicity.

The theoretical luminosity-specific PN number for B89 SSPs of different age, metallicity and mass-loss parameter is summarized in Figs 5 and 6, by matching the IFMR prescriptions according both to case (a) and (b), as in previous discussion. As expected, Fig. 5 shows that M_{core} is indeed the leading parameter constraining α ; note however the relevant difference between the IR83 and W00 models, with the latter reaching a fixed core mass at younger age, which corresponds to a brighter SSP luminosity. Compared to IR83, therefore, the W00 IFMR predicts in general a lower value of α for fixed value of M_{core} .

In this framework, the role of other SSP distinctive parameters, like metallicity and mass loss, only enters at a later crucial stage of the analysis, when tuning up the clock that links M_{core} to SSP age. This is displayed in Fig. 6, where the theoretical evolution of α is traced for SSPs spanning the full range of metal abundances and Reimers η parameter. Again, the IR83 $\eta = 0.3$ and 0.5 cases and the W00 IFMR are compared in the figure. When the variation of α is predicted as a function of the SSP age, the W00 model leads to a systematically higher PN number per unit SSP luminosity, compared to the IR83 case, due to a lower value of PAGB core mass assumed.

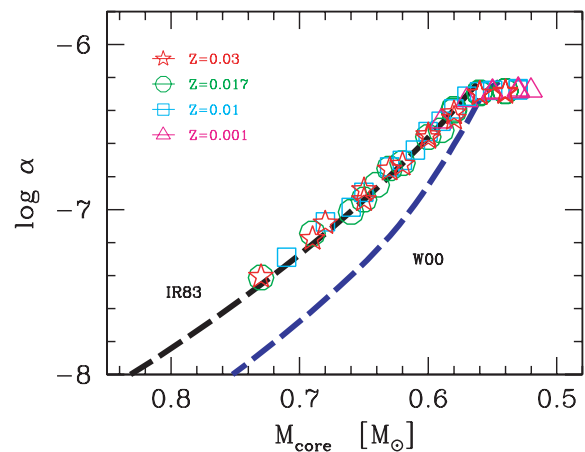


Figure 5. The luminosity-specific PN number for SSP models of Table 1 (both for $\eta = 0.3$ and 0.5 and different metallicity, as reported top left) compared to the PAGB stellar core mass. Overplotted are also the expected calibration assuming the theoretical IFMR of IR83 and the empirical one from W00, as labelled. Note the clean relationship in place, with M_{core} being the leading parameter to constrain α .

³ From the physical point of view, this would correspond to the He+H double-shell burning regime for low- and intermediate-mass stars.

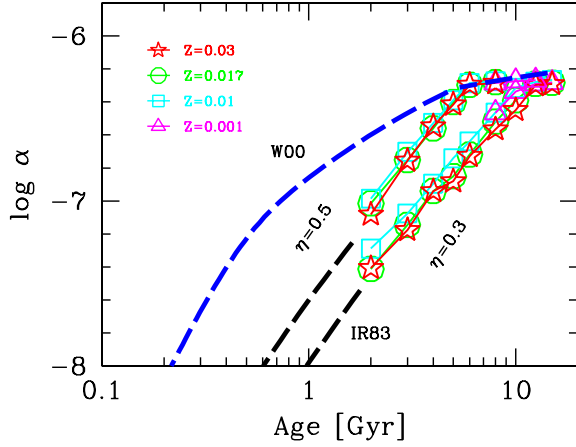


Figure 6. Theoretical time evolution of the luminosity-specific PN number for SSP models of Table 1 (both for $\eta = 0.3$ and 0.5 and the different metallicity values, as labelled top left on the plot) compared to the expected calibrations assuming the theoretical IFMR of IR83 and the empirical one from W00.

A summary of our calculations is reported in Table 1. A Salpeter IMF was adopted in the models, but a change in the power-law index with respect to the canonical value of $s = 2.35$ can easily be accounted for, following equation (4):

$$\Delta \log \alpha = \log \left(\frac{\alpha_s}{\alpha_{\text{Sal}}} \right) = \log \left(\frac{B_s}{B_{\text{Sal}}} \right) = \log \left(\frac{L_s}{L_{\text{Sal}}} \right). \quad (11)$$

This implies that, for a giant-dominated SSP ($s = 1.35$), $\log \alpha$ is ~ 0.04 dex higher, and the opposite happens for a dwarf-dominated SSP ($s = 3.35$), for which $\log \alpha$ is ~ 0.10 dex lower than for the Salpeter case (see Fig. 1).

The effect of enhanced mass loss on the Fig. 6 models can be quantified in roughly $\Delta \log \alpha \simeq +0.4$ dex for a change of η from 0.3 to 0.5 and fixed SSP age. This is a consequence of a lower core mass and a correspondingly slower PAGB evolution (see footnote 1), recalling that $\Delta \log \alpha = \Delta \log \tau_{\text{PAGB}}$.

A different value for the evaporation time-scale directly reflects on α_{max} . From equation (10), as $\Delta \log \alpha_{\text{max}} = \Delta \log \tau_{\text{dyn}}$, one has for instance that $\Delta \log \alpha_{\text{max}} \simeq -0.18$ dex when τ_{dyn} is decreased, say, to 20 000 yr.

Given the extreme uncertainty of theory in quantitatively assessing the PAGB transition time, in our SSP models we do *not* explicitly account for the quick drop of luminosity-specific PN number for the $0.52 M_{\odot} \lesssim M_{\text{core}} \lesssim 0.55 M_{\odot}$ PAGB core mass range. Operationally, as far as the PN evolutionary regime is driven by τ_{dyn} , we neglect the τ_{H} contribution and simply assume $\alpha = \alpha_{\text{max}}$,⁴ while for $M_{\text{core}} \leq 0.52 M_{\odot}$ no PN events are expected to occur at all and $\alpha = 0$. This crude simplification has negligible consequences when modelling late-type galaxies, while the evolution in the $0.52 \lesssim M_{\text{core}} \lesssim 0.55 M_{\odot}$ mass range becomes important for early-type galaxy models, as we shall discuss in more detail in Section 5.

As a concluding remark, we must also recall that α vanishes for SSP ages $t \lesssim 10^8$ yr, when the prevailing high-mass stars of $5\text{--}7 M_{\odot}$ or higher override the PN phase and end up their evolution as supernovae.

⁴ In this case, an upper limit is marked for α in Table 1.

3 THE LUMINOSITY-SPECIFIC PN NUMBER IN GALAXIES

The evolutionary properties of PNe in SSPs are the basis for extending the analysis to a wider range of star formation histories, as it happens in real galaxies. We use the template galaxy models developed by Buzzoni (2002, 2005), which ensure a self-consistent treatment of the PN evolution and the photometric properties of the stellar populations in the parent galaxy. In this framework, colours and morphological features along the Hubble sequence for early- and late-type systems were reproduced tracing the individual luminosity contribution for the bulge, disk and halo component (see Buzzoni 2002, 2005, for additional details).

Following Section 2.4, the PN evolution has been implemented in the models in a semi-analytical way, by fitting the SSP data in Table 1 for the $\eta = 0.3$ and 0.5 cases, and for the W00 empirical IFMR. The whole data grid can be fitted within a 6 per cent formal uncertainty in the value of α [i.e. $\sigma(\log \alpha) = \pm 0.025$ dex] over the age/metallicity range by

$$\log \alpha' = (1.52 - 0.07z) \log t_9 - 0.07 \log^2(3.4z) - 0.1/t_9 + 2.0(\eta - 0.3) - 7.80, \quad (12)$$

where t_9 is the SSP age in Gyr, and $z = Z/Z_{\odot}$. For solar metallicity, equation (12) reproduces the IR83 calibration over the extended age range of Table 1. Similarly, a fit to the W00 relation is

$$\log \alpha' = -0.6(\log t_9 - 1)^2 - 6.27. \quad (13)$$

In addition, we also assume that

$$\alpha = \begin{cases} \min[\alpha', \alpha_{\text{max}}] & \text{for } t_9 \geq 0.1, \\ 0 & \text{for } t_9 < 0.1, \end{cases} \quad (14)$$

where α_{max} is given by equation (10).

The absolute number of PNe in a SSP of total (bolometric) luminosity L_{SSP} simply becomes $N_{\text{PN}}(\text{SSP}) = \alpha L_{\text{SSP}}$, and for a star-forming galaxy of age t , we write

$$\mathcal{N}_{\text{PN}}(t) = \int_0^t \alpha(\tau) L_{\text{SSP}}(\tau) \text{SFR}(t - \tau) d\tau. \quad (15)$$

Therefore, the global luminosity-specific PN number for the galaxy stellar population can be computed as

$$\alpha(t) = \frac{\mathcal{N}_{\text{PN}}(t)}{L_{\text{gal}}} = \frac{\int_0^t \alpha(\tau) L_{\text{SSP}}(\tau) \text{SFR}(t - \tau) d\tau}{\int_0^t L_{\text{SSP}}(\tau) \text{SFR}(t - \tau) d\tau}. \quad (16)$$

The results for the whole Hubble sequence, from type E to Im, are summarized in Fig. 7 and Table 2 for the $\eta = 0.3$ case ($\alpha_{0.3}$ in the table) and the W00 IFMR (α_{W}). In Table 2, we provide also the integrated $B - V$ colour for the parent galaxy, and the absolute bolometric luminosity of the system, assuming a total stellar mass of $M_{\text{gal}} = 10^{11} M_{\odot}$ at 15 Gyr (see Buzzoni 2005, for a detailed definition of this quantity).⁵

⁵ The Buzzoni (2005) galaxy models are computed with a standard mass-loss parameter $\eta = 0.3$, and the integrated magnitudes and colours reported in Table 2 refer to this case. The effect on galaxy $B - V$ by adopting the alternative W00 IFMR can be estimated in $\Delta(B - V) \simeq -0.02$ mag, that is with a little shift toward bluer colours (see e.g., the calibration from fig. 28 in Buzzoni 1995). The value reported in Table 2 for $\log \alpha_{\text{W}}$ should also be increased by an additional $\Delta \log \alpha_{\text{W}} \simeq +0.04$ dex if one takes into account slightly fainter galaxies (some ~ 10 per cent in bolometric luminosity) in the W00 framework.

Table 1. Luminosity-specific PN number for Salpeter SSPs^a.

Age (Gyr)	Metallicity (Z)										
	0.001	0.01	0.017 $\eta = 0.3$	0.03	IR83	0.001	0.01	0.017 $\eta = 0.5$	0.03	IR83	W00
0.1	–	–	–	–	–10.33	–	–	–	–	–9.71	–8.71
0.5	–	–	–	–	–8.57	–	–	–	–	–8.16	–7.22
1.0	–	–	–	–	–7.98	–	–	–	–	–7.60	–6.86
2.0	–	–7.29	–7.41	–7.41	–7.45	–	–6.99	–7.02	–7.08	–7.11	–6.60
3.0	–	–7.08	–7.15	–7.18	–7.17	–	–6.70	–6.75	–6.76	–6.85	–6.47
4.0	–	–6.90	–6.94	–6.94	–6.98	–	–6.53	–6.56	–6.55	–6.68	–6.38
5.0	–	–6.74	–6.85	–6.88	–6.84	–	–6.39	–6.40	–6.42	–6.54	–6.32
6.0	–	–6.64	–6.72	–6.73	–6.73	–	–6.29	–6.30	–6.30	–6.45	–6.30
8.0	–6.47	–6.46	–6.52	–6.57	–6.56	–6.29	≤ -6.28	≤ -6.28	≤ -6.29	–6.28	–6.27
10.0	–6.34	–6.31	–6.39	–6.45	–6.44	≤ -6.27	no PNe ^b			–6.27	–6.27
12.5	–6.29	–6.28	–6.29	–6.30	–6.31					–6.27	–6.27
15.0	≤ -6.28	≤ -6.27	≤ -6.28	≤ -6.29	–6.27					≤ -6.27	≤ -6.27

^aThe listed quantity is $\log \alpha = \log N_{\text{PN}} - \log (L_{\text{SSP}}/L_{\odot})$.

^bPNe not expected to form for these age/metallicity combinations as $M_{\text{PAGB}} \leq 0.52 M_{\odot}$.

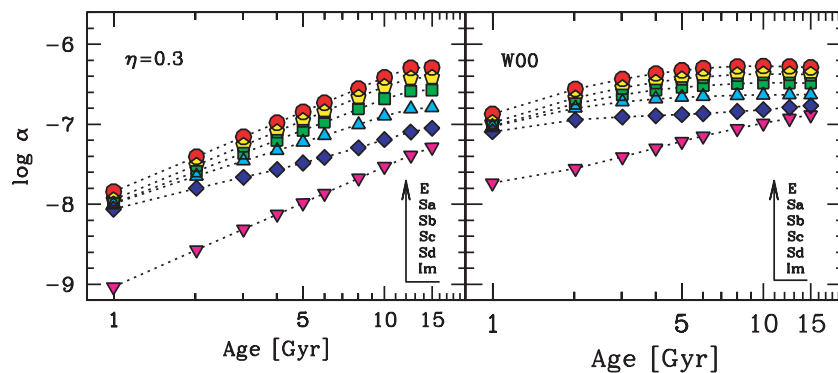


Figure 7. Theoretical time evolution of the luminosity specific PN density (α) for the Buzzoni (2005) template galaxy models along the whole E-Sa-Sb-Sc-Sd-Im Hubble morphological sequence. Models in left-hand panel assume an IFMR as from the standard mass-loss parameter $\eta = 0.3$, while those in the right-hand panel rely on the empirical relation from W00. Note, in the latter case, the much shallower evolution of α . In the two panels, bulge-dominated spirals tend to approach the evolution of ellipticals at early epochs due to the increasing bulge contribution to the global galaxy luminosity.

The two evolutionary scenarios produce large differences in $\alpha(t)$ for the Hubble morphological types: the W00 model predicts larger PN populations and a shallower time dependence for α than for the $\eta = 0.3$ case. The effects are larger for late-type galaxy models, where the impact of the different IFMR details on intermediate- and high-mass stars is stronger. Also, the nucleated late-type galaxies (types Sa \Rightarrow Sd) approach the evolution of ellipticals at early epochs. As discussed in some detail in Buzzoni (2005), this effect is due to the prevailing photometric contribution of the bulge stellar component, when $t \rightarrow 0$.

The general prediction from these models is that α is expected to decrease in young and/or star-forming galaxies, compared to more ‘quiescent’ early-type systems as a consequence of a smaller population of PNe embedded in a higher galaxy luminosity per unit mass (i.e. a lower M/L ratio).

3.1 Comparing with the observations: PN luminosity function and completeness corrections

The empirical evidence, from the 5007 \AA [OIII] PN luminosity distribution, indicates a nearly constant value for the bright cut-off magnitude (M^*) of the PNLF. This feature is actually found to be nearly invariant with galaxy type and age and, as suggested by Jacoby

(1989), can be effectively used as a standard candle to determine extragalactic distances.

When the emission-line fluxes are converted into equivalent V magnitudes via the formula

$$m_{[\text{OIII}]} = -2.5 \log F_{[\text{OIII}]} - 13.74 \quad (17)$$

(Jacoby 1989), the PNLF takes the shape of a double-exponential function (Ciardullo et al. 1989) of the form

$$\log N(M) = 0.133 M + \log [1 - e^{3(M^* - M)}] + \text{const}, \quad (18)$$

with the bright cut-off magnitude placed at $M^* = -4.47$ mag plus a little metallicity correction, that scales with PN Oxygen abundance, such as

$$\Delta M^* = 0.928 [O/H]^2 + 0.225 [O/H] + 0.014 \quad (19)$$

(Dopita, Jacoby & Vassiliadis 1992). After correction, the inferred PN distances in external galaxies are consistent within 0.1 dex with those obtained using the Cepheids method for a large observed sample of galaxies and galaxy types (Ciardullo et al. 2002a).

There is no theoretical explanation of this ‘universal’ property of the PN distribution, although it has been questioned (e.g. Méndez et al. 1993) that it might depend on the sample size, being therefore a mere statistical effect. Furthermore, on the theoretical side, some

Table 2. The luminosity-specific PN number for template galaxy models^a.

Age (Gyr)	M_{bol}	$B - V$	$\log \alpha_{03}$	$\log \alpha_{\text{W}}$	M_{bol}	$B - V$	$\log \alpha_{03}$	$\log \alpha_{\text{W}}$	M_{bol}	$B - V$	$\log \alpha_{03}$	$\log \alpha_{\text{W}}$
	E				Sa				Sb			
1.0	-23.10	0.66	-7.84	-6.87	-23.22	0.58	-7.94	-6.98	-23.11	0.55	-7.99	-7.02
2.0	-22.48	0.72	-7.40	-6.56	-22.67	0.63	-7.51	-6.67	-22.66	0.58	-7.59	-6.74
3.0	-22.13	0.76	-7.16	-6.43	-22.36	0.65	-7.27	-6.54	-22.42	0.59	-7.36	-6.63
4.0	-21.89	0.79	-6.98	-6.36	-22.14	0.67	-7.09	-6.47	-22.25	0.60	-7.20	-6.57
5.0	-21.70	0.81	-6.84	-6.32	-21.97	0.69	-6.95	-6.43	-22.13	0.61	-7.08	-6.54
6.0	-21.54	0.83	-6.73	-6.30	-21.84	0.70	-6.84	-6.41	-22.03	0.62	-6.97	-6.52
8.0	-21.30	0.86	-6.55	-6.28	-21.62	0.72	-6.66	-6.38	-21.88	0.63	-6.81	-6.49
10.0	-21.11	0.88	-6.41	-6.27	-21.45	0.74	-6.53	-6.37	-21.76	0.63	-6.68	-6.48
12.5	-20.92	0.90	-6.29	-6.28	-21.29	0.75	-6.42	-6.37	-21.65	0.64	-6.58	-6.48
15.0	-20.76	0.92	-6.29	-6.29	-21.15	0.76	-6.41	-6.38	-21.57	0.65	-6.57	-6.49
	Sc				Sd				Im			
1.0	-22.80	0.55	-7.99	-7.03	-22.12	0.51	-8.06	-7.09	-20.29	0.30	-9.03	-7.73
2.0	-22.47	0.55	-7.65	-6.80	-22.05	0.48	-7.80	-6.94	-21.06	0.34	-8.57	-7.55
3.0	-22.34	0.54	-7.46	-6.72	-22.11	0.46	-7.66	-6.91	-21.49	0.36	-8.31	-7.41
4.0	-22.26	0.54	-7.33	-6.68	-22.18	0.46	-7.56	-6.89	-21.80	0.38	-8.13	-7.30
5.0	-22.22	0.54	-7.22	-6.66	-22.25	0.46	-7.48	-6.88	-22.04	0.39	-7.98	-7.21
6.0	-22.19	0.54	-7.14	-6.65	-22.32	0.46	-7.41	-6.87	-22.24	0.40	-7.86	-7.15
8.0	-22.15	0.54	-7.00	-6.64	-22.44	0.47	-7.29	-6.84	-22.55	0.42	-7.67	-7.05
10.0	-22.13	0.55	-6.90	-6.63	-22.54	0.48	-7.19	-6.82	-22.79	0.43	-7.53	-6.99
12.5	-22.12	0.55	-6.81	-6.63	-22.64	0.49	-7.10	-6.79	-23.03	0.45	-7.39	-6.93
15.0	-22.11	0.56	-6.79	-6.63	-22.73	0.49	-7.05	-6.77	-23.23	0.46	-7.29	-6.88

^aModels are for a Salpeter IMF;

$\log \alpha_{03}$ = luminosity-specific PN number assuming a theoretical IFMR with a fixed Reimers mass-loss parameter $\eta = 0.3$;

$\log \alpha_{\text{W}}$ = luminosity-specific PN number assuming an empirical IFMR according to Weidemann (2000).

change of M^* with the age of the PN parent stellar population should be expected, its precise amount strongly depending, however, on the model assumptions (see especially Marigo et al. 2004, for the most striking results on this line).

While the bright end of the PNLF has been studied in a large number of galaxies, not much is known about the PNLF shape at fainter magnitudes, as most LG surveys are complete down to 4 mag from the bright cut-off luminosity (Corradi & Magrini 2006), and this limit becomes obviously brighter for more distant systems. This implies a still large uncertainty in the extrapolation from the *observed* number of PNe to the *whole* PN population size, through equation (18). In particular, there is evidence of a dip in the PNLF of the Small Magellanic Cloud (SMC) (Jacoby & De Marco 2002) and M33 (Magrini et al. 2000; Ciardullo et al. 2004) at 4 and 2.5 mag, respectively, below the bright cut-off (cf. Fig. 8, dashed curve in the bottom panel), but this is not observed in the M31 bulge (Ciardullo et al. 2002a). The presence of the dip might depend on the galaxy star formation history (through the age distribution of PN progenitors), possibly witnessing the presence of a significant component of young stars (Ciardullo et al. 2004; Marigo et al. 2004).

According to Ciardullo et al. (1989) and Jacoby (1980), the faint-end tail of the standard PNLF agrees with the theoretical luminosity function of Henize & Westerlund (1963), in which a PN is modelled as a uniformly expanding homogeneous gas sphere ionized by a non-evolving central star. The number of nebulae in each luminosity interval should then be proportional to the PN lifetime spent within that luminosity bin. For a global PN lifetime of 30 000 yr, Henize & Westerlund (1963) predict that faintest PNe should locate about 8 mag below M^* .

Deep observations in the SMC (Jacoby & De Marco 2002; Jacoby 2006), reaching more than 6 mag below the bright cut-off, show a significant decline of the number of PNe compared to what predicted by the double-exponential formula. Clearly, a more extended sample from other nearby galaxies at comparable magnitude depth would

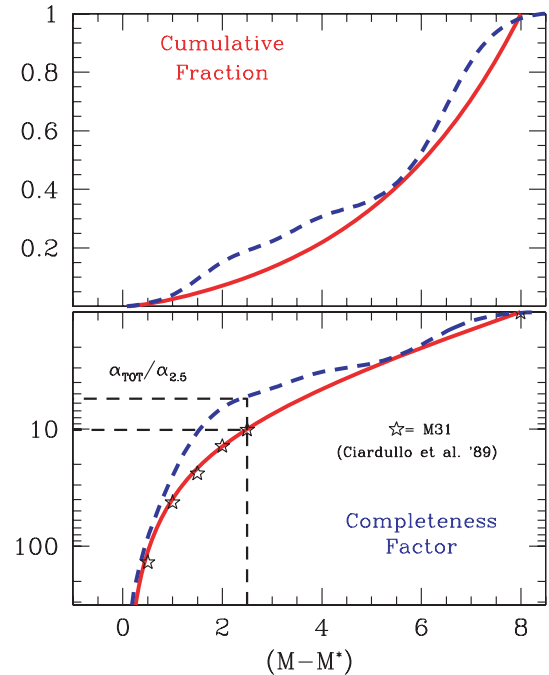


Figure 8. Upper panel: the cumulative fraction of PNe in the different magnitude bins with respect to the luminosity-function bright cut-off (M^*) for the double-exponential fit of the PNLF, as in equation (18) (solid curve) and for the empirical SMC luminosity function according to Jacoby (2006) (dashed curve). Lower panel: completeness factor ($CF = N_{\text{tot}}/N_{(M-M^*)}$) for the same calibrations as in the upper panel. Also reported are the Ciardullo et al. (1989) data for M31 (star markers), and the relevant correction factor for the $\alpha_{2.5}$ parameter. For better convenience, data are also listed in Table 3.

Table 3. The PNLF.

$M - M^*$ (mag)	Cumulative fraction		Completeness factor	
	Standard	SMC	Standard	SMC
0.0	0	0	∞	∞
0.5	0.009	0.013	113	78.3
1.0	0.025	0.042	39.8	23.7
1.5	0.046	0.097	21.6	10.3
2.0	0.071	0.155	14.1	6.46
2.5	0.100	0.193	9.99	5.19
3.0	0.134	0.225	7.46	4.44
3.5	0.173	0.269	5.76	3.72
4.0	0.219	0.310	4.56	3.23
4.5	0.273	0.336	3.66	2.98
5.0	0.336	0.366	2.98	2.73
5.5	0.409	0.427	2.45	2.34
6.0	0.494	0.535	2.03	1.87
6.5	0.593	0.692	1.69	1.44
7.0	0.708	0.845	1.41	1.18
7.5	0.843	0.941	1.19	1.06
8.0	1	1	1.00	1.00

be required to better assess this important problem. Unfortunately, in case of late-type galaxies, the [O III] PN detection is not quite a simple task; due to the ongoing star formation, only a very small fraction of the [O III] emission-line sources in spirals and irregulars is represented by genuine PNe, in most cases counts are affected by H II regions and supernova remnants. Identification of PNe in LG galaxies requires additional constraints, such as point-like on-line emission combined with a non-detection in the off-line continuum, and a stronger [O III] emission compared to H α and/or [N II] narrow-band luminosity.⁶ In addition, disk regions can be heavily obscured by dust, and the sample completeness with respect to the parent stellar population light may also be affected.

A comparison of the Jacoby (2006) updated SMC PNLF with the standard double-exponential function, as in equation (18), is proposed in Table 3 and Fig. 8. If the faint-end tail of the PNLF indeed occurs at 8 mag down from the bright cut-off, then one can determine the fraction of PNe in the brightest 2.5-mag range, and define a parameter $\alpha_{2.5}$ as the luminosity-specific number of PNe with $M - M^* \leq 2.5$. Fig. 8 and Table 3 show that such bright nebulae represent a fraction between 10 and 20 per cent of the total PN population.

As we will see in the following sections, the definition of $\alpha_{2.5}$, which includes only the brighter PNe, makes the comparison with observations in external galaxies easier. For our discussion, we assume a simple relation such as $\alpha = 10 \times \alpha_{2.5}$, according to the standard PNLF (column 4 in Table 3). This normalization is correct if the double-exponential PNLF formula applies, and there are no PNe 8-mag fainter than the bright cut-off.

3.1.1 Galaxy bolometric correction

To compare observations and model predictions for the luminosity-specific PN number in external galaxies, we need to convert the

⁶ A stronger [O III] emission versus H α is found to be an excellent diagnostic tool for bright PNe (Ciardullo et al. 2004), while a reversed trend is likely to be expected for the faintest nebulae (Magrini et al. 2000). See, for instance, Arnaboldi et al. (2003) and Corradi et al. (2005) for further diagnostic plots in the emission-line narrow-band colour domain.

monochromatic galaxy luminosity to bolometric. One can use the Johnson V or B magnitudes for galaxy photometry, corrected for the distance modulus such as to match the absolute scale, and usually complemented with a (rough) estimate of the colour excess, $E(B - V)$, to account for Galactic reddening.

Given the (reddening-corrected) values of M_B and M_V , the required transformations to provide L_{gal} in equation (16) are the following:

$$L_{\text{gal}} = \begin{cases} 10^{-0.4(M_B - 5.41)} 10^{-0.4(BC_B + 0.69)}, \\ 10^{-0.4(M_V - 4.79)} 10^{-0.4(BC_V + 0.07)}, \end{cases} \quad (20)$$

where BC_B and BC_V are the bolometric corrections to the B and V band, respectively; according to B89, in our notation the Sun has $M_{\odot}^{\text{bol}} = +4.72$ mag, $BC_{\odot}^V = -0.07$ mag and $BC_{\odot}^B = -0.69$ mag. A direct estimate of the bolometric correction from the galaxy observations is not a straightforward task, and the alternative way is to rely on models.

Fig. 9 shows the trend of the B and V bolometric correction for the Buzzoni (2005) galaxy templates over the age range from 1 to 15 Gyr. One sees that a simple and convenient solution, within a 10 per cent internal accuracy (i.e. ± 0.1 mag) in the transformation, can be found for the V -band correction, assuming a fixed value $BC_V = (\text{Bol} - V) = -0.85$ mag all over the relevant range of galaxy types and age. A suitable estimate for the B -correction is $BC_B = (\text{Bol} - V) - (B - V) = -0.85 - (B - V)$ mag.

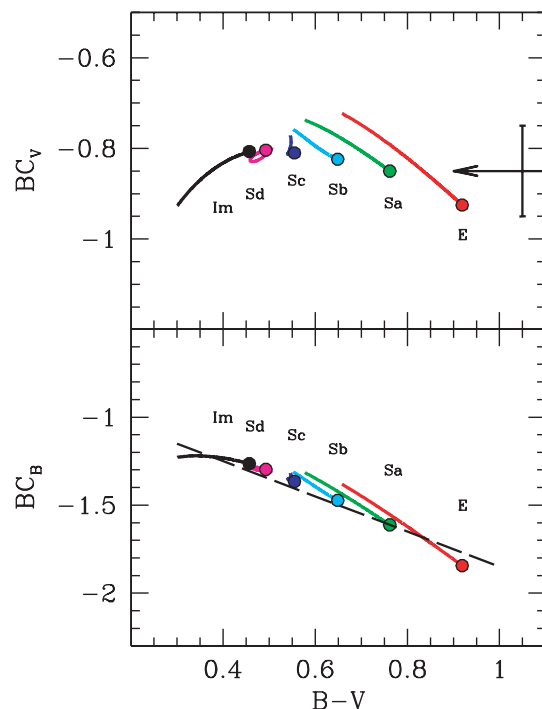


Figure 9. The expected bolometric correction for theoretical template galaxy models according to Buzzoni (2005). The models for different morphological type span the age range from 1 to 15 Gyr (the latter limit being marked by the solid dot on each curve). Bolometric correction refers to the V (upper panel) and B band (lower panel). A value of $(\text{Bol} - V) = BC_V = -0.85$ mag can be taken as a representative correction for the whole galaxy types within a 10 per cent uncertainty, as shown by the arrow on the upper plot. This also translates into $BC_B \simeq -0.85 - (B - V)_{\text{gal}}$ for the B -band correction, as displayed by the dashed line in the lower panel.

Table 4. The PN census in the LG galaxies^a.

Name	Morph. type	Distance (Mpc)	M_B	$(B - V)_0$	$[O/H]^b$	Observed no. of PNe	Completeness limit $M_{\text{lim}} - M^*$	N_{tot}^c		$\log \alpha \pm \sigma$	Ref.
								Standard	SMC		
M31 (all)	Sb	0.76	-21.55	0.68 ± 0.02	+0.1	~2700		19000 ± 8000			(1)
M31 (bulge)			-18.01	0.95 ± 0.02^d		94	2.5	940 ± 97	497 ± 51	$-6.94^{0.15}_{0.22}$	(2)
Milky Way	Sbc	0.01	-20.80	0.63^e	-0.2	~2000		25000 ± 19000		$-6.40^{0.25}_{0.63}$	(3), (4)
M 33	Scd	0.80	-18.74	0.47 ± 0.02	-0.5	152	2.6	765 ± 85	415 ± 46	$-7.13^{0.14}_{0.22}$	(5)
LMC	SBm	0.050	-17.93	0.44 ± 0.03	-0.52	~1000	~7.0				(5)
						~350	~5.0	1040 ± 60	960 ± 50	$-6.57^{0.04}_{0.04}$	(6)
SMC	SBm	0.060	-16.24	0.41 ± 0.03	-0.84	105	6.0		167 ± 19	$-6.67^{0.05}_{0.05}$	(7),(6)
NGC 205	E5	0.76	-15.96	0.82 ± 0.05	-0.3	35	3.5	134 ± 28	87 ± 18	$-6.88^{0.15}_{0.22}$	(2)
M 32	E2	0.76	-15.93	0.88 ± 0.01	-0.58	30	2.4	186 ± 44	97 ± 23	$-6.77^{0.18}_{0.31}$	(3), (4)
IC 10	Im	0.66	-15.57	0.58 ± 0.05	-0.7	16	2.0	153 ± 46	72 ± 22	$-6.59^{0.20}_{0.40}$	(5)
NGC 6822	Im	0.50	-15.22	0.47 ± 0.15^e	-0.62	17	3.5	74 ± 21	48 ± 13	$-6.69^{0.16}_{0.27}$	(6)
NGC 185	E3	0.66	-14.90	0.73 ± 0.01	-1.0	5	2.7	45 ± 20	25 ± 11	$-6.88^{0.22}_{0.45}$	(2)
NGC 147	E5	0.66	-14.48	0.78 ± 0.05		9	3.9	29 ± 12	20 ± 8	$-6.91^{0.19}_{0.34}$	(3), (4)
Sex A	Im	0.86	-13.02	0.37 ± 0.08	-1.32	1	1.9	16 ± 16	7 ± 7	$-6.38^{0.30}_{\infty}$	(5)
Sex B	Im	0.86	-12.96	0.51 ± 0.03	-0.75	5	3.0	37 ± 17	22 ± 10	$-6.10^{0.21}_{0.44}$	(6)
Leo A	Im	0.69	-11.36	0.31 ± 0.08	-1.51	1	3.0	8 ± 8	5 ± 5	$-5.99^{0.30}_{\infty}$	(7)

References: (1) Merrett et al. (2003); (2) Ciardullo et al. (1989); (3) Jacoby (1980); (4) Alloin et al. (1976); (5) Reid & Parker, private communication; (6) Jacoby (2006); (7) Jacoby & De Marco (2002).

^aGalaxy morphological types and $(B - V)$ colours are from the RC3 catalog (de Vaucouleurs et al. 1991), distances and metallicities from Corradi & Magrini (2006), absolute B magnitudes, M_B , from Karachentsev (2005) rescaled to the Corradi & Magrini (2006) distance modulus. Both $(B - V)$ and M_B quantities are reddening- and inclination-corrected according to the corresponding literature sources.

^bAdopted PN Oxygen abundance, $[O/H] = \log(O/H) - \log(O/H)_{\odot} = 8.87$ (Grevesse, Noels & Sauval 1996).

^cPN population size within 8 mag from the PNLf bright-end tail, inferred according to two different extrapolation methods: Standard: empirical PNLf from Jacoby (1989), as in Table 3 (columns 2 and 4), corrected for metallicity after Dopita et al. (1992); SMC: using the Jacoby (2006) observed SMC PNLf (see columns 3 and 5 in Table 3), and correcting for metallicity as for the ‘Standard’ case.

^dData from HyperLeda Lyon.

^eThe $(B - V)$ estimate for the Milky Way is from the Robin et al. (2003) synthetic model, as quoted by Boissier & Prantzos (1999).

4 COMPARISON WITH OBSERVED PN POPULATIONS

4.1 The Local Group PN census

The LG galaxies have been extensively searched for PNe since the discovery of five PNe in M 31 by Baade (1955). Recent surveys including all LG galaxies with $\log(L_B/L_{\odot}) > 6.7$, provide a comprehensive view of LG PN population which can be used as a first comparison for our population synthesis models. An updated list of the number of PNe known in the LG can be found in the work of Corradi & Magrini (2006). While PNe have been found in 20 LG galaxies, the survey completeness and photometric accuracy are not good enough to allow a confident estimate of their global population in all of them.

In Table 4, we therefore summarize the updated information for the PN census only for those LG galaxies whose survey completeness limit (and the number of PNe within it) is known. Many of the data come from the so-called Local Group Census Project (see e.g. Corradi et al. 2005, and references therein); other sources are indicated in the table.

From these data, we have estimated the total PN population size of these galaxies (N_{tot} in Table 4) in two ways, to account for the uncertainty in our knowledge of the shape of the PNLf at faint magnitudes. First, for each galaxy the magnitude difference between the completeness limit of the survey and the expected apparent mag-

nitude of the PNLf cut-off, m^* , was computed. The value of m^* is determined assuming $M^* = -4.47$, the metallicity correction in equation (19) with the value of $[O/H]$ as reported in column 6 of the table, and the distances as in Corradi & Magrini (2006) (listed again in column 3 here). The observed number of PNe within the completeness limit has then been extrapolated 8 mag down the PNLf cut-off using the empirical formula in equation (18), as reported in Table 3; resulting figures are listed in column 9 of Table 4. The total PN population size was also estimated rescaling the *observed* PNLf of the SMC (Jacoby & De Marco 2002, see column 5 of Table 3), which is complete 6 mag down the cut-off, and assuming a ~50 per cent incompleteness for the next magnitude bin, consistent with recent deeper observations (Jacoby 2006). The corresponding total PN population estimated for the LG galaxies is indicated in column 10 of Table 4.

For the SMC, the adopted PN population is the number estimated by Jacoby & De Marco (2002), plus some 20 per cent to include the faintest PNe as suggested by recent observations (Jacoby 2006). The Large Magellanic Cloud (LMC) population size is determined using approximate figures of the observed number of PNe and the depth of the discovery surveys, according to Jacoby (2006). For M 31, data for a relatively dust-free region in the bulge (Ciardullo et al. 1989) were adopted; the local number of PNe was then rescaled to the whole galaxy luminosity. The latter value represents an estimate of the global population, and the derived value of α reported in Table 4 is in fact representative of the bulge evolutionary environment. Finally,

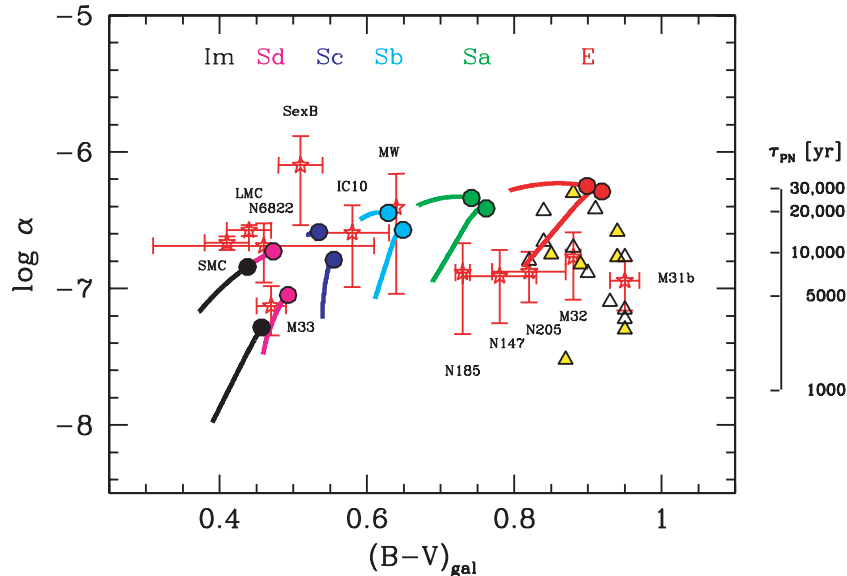


Figure 10. A comprehensive overview of the luminosity-specific PN number in LG galaxies (star markers) and external ellipticals from Table 5 (solid triangles) and Table 6 (open triangles). PN data for local galaxies are from Table 4, and are based on the ‘Local Group Census Project’ of Corradi et al. (2005). Also superposed on the plot, there are the Buzzoni (2005) template galaxy models, as summarized in Table 2. Galaxy evolution is tracked by models along the whole E-Sa-Sb-Sc-Sd-Im Hubble morphological sequence from 5 to 15 Gyr, with the latter limit marked by the big solid dots. Two model sequences are reported on the plot assuming an IFMR as from the standard case of a Reimers mass-loss parameter $\eta = 0.3$ (lower sequence), and from the empirical relation of W00 (upper sequence). For the W00 models, the relevant data of Table 2 have been corrected by $\Delta(B - V) = -0.02$ mag and $\log \alpha = \log \alpha_{W00} + 0.04$, according to the arguments of footnote 5. An indicative estimate of the mean representative PN lifetime (in years) is sketched on the right scale, according to equation (22).

the total PN population for the Milky Way in Table 4 is a conservative estimate from the data by Jacoby (1980) and Alloin, Cruz-González & Peimbert (1976).

The difference between the total PN population based either on the ‘standard’ or the ‘SMC’ PNLF is of a factor 2 or smaller. The derived value of α is reported in column 11 of Table 4, assuming for LG galaxies the $B - V$ colours from the RC3 catalog (de Vaucouleurs et al. 1991) and the absolute M_B magnitudes from Karachentsev (2005), converted to bolometric according to equation (20).⁷ The quoted error bars in the table are conservative estimates of the uncertainty of N_{tot} , which account for the difference between the ‘standard’ and ‘SMC’ PNLF extrapolated values.

The LG galaxy sample provides the natural benchmark to test our theoretical models over a range of evolutionary environments and star formation histories. Our predictions for the Buzzoni (2005) template galaxy models of Table 2 are compared in Fig. 10 with the LG data of Table 4 for a relatively old age range, from 5 to 15 Gyr, and mass-loss scenarios ($\eta = 0.3$ and W00).

The remarkable feature of the $\log \alpha$ plot, for the observed galaxies representative of the whole Hubble morphological sequence, is the fairly constant PN rate per unit galaxy luminosity. Data support an average rate between 1 and 6 PNe per $10^7 L_{\odot}$. Such a value is related to a narrow range of PAGB stellar core mass, according to the calibration of Fig. 5, with M_{core} less than 0.60–0.65 M_{\odot} .

There are at least three important consequences of this sharp mass distribution: (i) the mass-loss scenario supported by the observations

better agrees with the W00 IFMR, which implies a stronger mass loss for intermediate and high-mass stars compared to the standard scenario ($\eta \simeq 0.3$ –0.5) for Pop II stars as in Galactic globular clusters; (ii) according to Section 2.2, for a consistent fraction of the PN population in LG galaxies the inferred lifetime is constrained by the dynamical time-scale of nebula evaporation rather than the stellar core mass evolution; (iii) the latter evidence also supports a small dependence of α with time and distance (see right-hand panel of Fig. 7) pointing to a relatively ‘universal’ shape for the PNLF (but see, however, Section 5.2 for an important warning in this regard).

4.2 PN surveys in external galaxies

As discussed in Section 3.1, a complete survey of the PN population in late-type galaxies is often plagued by spurious detections caused by HII regions, SN remnants and, for galaxies at distances larger than 10 Mpc, by Ly α background galaxies at $z \simeq 3.13$, (see e.g. Ciardullo et al. 2002b; Arnaboldi 2004).

Current surveys only investigate the brightest magnitude bin of the PNLF, to measure the bright cut-off magnitude M^* and lead therefrom to galaxy distance (see, e.g. Ciardullo et al. 2002a, for a recent survey of six S0 and active, mostly Seyfert 2, spirals). The best samples of PNe in late-type systems still remain the ones for M 31 and M 33 (Magrini et al. 2000; Merrett et al. 2003; Ciardullo et al. 2004).

4.2.1 PN samples in early-type galaxies

The lack of active star formation and a negligible fraction of residual gas in early-type galaxies make the [O III] PN detection relatively straightforward across the whole galaxy body, excluding the innermost regions, where the galaxy spectral continuum is too bright.

⁷ To be consistent with the Corradi & Magrini (2006) survey and completeness correction, the Karachentsev (2005) absolute M_B magnitudes have been slightly rescaled to the Corradi & Magrini (2006) adopted galaxy distances, as reported in Table 4. Note, in addition, that both M_B and $(B - V)$ are reddening- and inclination-corrected values according to the original data sources.

Table 5. Recent additions to PN census in early-type galaxies.

Name	Morph. type ^a	Observed no. of PNe	Comp. limit $M - M^*$	N_{tot}^b	$\log \alpha$	Ref.
NGC 1316	S0	43	1.0	1720 ± 262	-7.50 ± 0.07	Arnaboldi et al. (1998)
NGC 1344	E5	197	1.0	2300 ± 47	-6.75 ± 0.02	Teodorescu et al. (2006)
NGC 1399	E1	37	1.0	1480 ± 243	-7.30 ± 0.07	Arnaboldi et al. (1994)
NGC 3115	S0	61	1.0	2440 ± 312	-6.59 ± 0.05	Ciardullo et al. (2002a)
NGC 3379	E1	109	2.0	1535 ± 104	-6.77 ± 0.03	Romanowsky et al. (2003)
NGC 4697	E6	535	2.5	3500 ± 231	-6.82 ± 0.03	Méndez et al. (2001)
NGC 5128	S0	431	2.5	4300 ± 207	-6.30 ± 0.02	Hui et al. (1993)

^aFrom the RC3 catalog (de Vaucouleurs et al. 1991).

^bPN population size within 8 mag from the PNLF bright-end cut-off, inferred according to standard PNLF, as in Table 3 (columns 2 and 4).

However, only low-mass ellipticals and dwarf spheroidals can be found among the LG galaxy population and, with the exception of NGC 5128 (Cen A) at 3.5 Mpc, the nearest normal and/or giant ellipticals are at 10 Mpc or further. At these distances, the typical [O III] magnitudes are in the range 26–27 mag or fainter, and spectroscopic-confirmed PN samples are usually limited to $M \lesssim M^* + 1.0$, with only few good cases observed in slitless spectroscopy. Hopefully, larger PN samples in early-type galaxies will soon be available with the dedicated PN.S spectrograph operating at the William Herschel Telescope at La Palma (Douglas et al. 2002).

A comprehensive collection of PN data for dwarfs, giant elliptical and S0 galaxies in the LG, Leo group and the Virgo cluster can be found in Hui et al. (1993), comparing original observations of NGC 5128 with the value of $\alpha_{2.5}$ for a sample of 13 early-type galaxies plus the bulge of M 31. An updated census for some of these objects, plus additional results from deeper surveys for a few more galaxies are listed in Table 5. In column 4, we report the total number of detected PNe (at all magnitudes) together with the completeness limit of the survey, ($M - M^*$), and the inferred number of the global PN population on the sampled galaxy region (with its Poissonian error estimate), by assuming a standard PNLF down to $M = M^* + 8.0$ mag. The value of α is then computed by normalizing to the sampled galaxy luminosity, according to the original data sources in the literature.

For the data of Table 5 and the Hui et al. (1993) sample, we collected, in Table 6, supplementary dynamical and photometric information from Burstein et al. (1988), the RC3, NED and HyperLeda on-line data bases. Two LG galaxies were also added to the sample, including the dwarf satellite ellipticals of M 31 (i.e. NGC 205 and M 32), and the bulge data for M 31 itself. This whole sample of early-type galaxies is displayed in Fig. 10, matching the LG data and the Buzzoni (2005) template galaxy models.

As pointed out by Hui et al. (1993), in the plot of Fig. 10 one can notice a sharp decrease of the luminosity-specific PN number in early-type galaxies compared with the theoretical predictions of our E-galaxy model and the empirical estimate of α for the Milky Way and other nearby spirals. In addition, following Peimbert (1990) and Hui et al. (1993), the figure also reports a *clear trend of α with galaxy colour, with a poorer PN population (per unit bolometric luminosity) in redder ellipticals*. So far, this trend has not received a satisfactory explanation.

5 THE PN POPULATION IN ELLIPTICALS

From the definition of α in equation (3), a lower value of the luminosity-specific PN number corresponds to a shorter PN life-

time. If 30 000 yr is a reasonable value for τ_{PN} in the most PN-rich galaxies, then

$$\frac{\alpha}{\alpha_{\text{max}}} \approx \frac{\tau_{\text{PN}}}{30\,000}. \quad (21)$$

For a low value of α , like for instance in NGC 1316 or NGC 1399, one leads therefore to a lifetime of 3000–5000 yr for the galaxy PN population (see the right-scale calibration in Fig. 10).⁸ The value of τ_{PN} linked to the observed value of α in equation (21) must, however, be regarded as an average on the PAGB core mass distribution, which cannot be determined observationally in systems other than the Milky Way (e.g. Zhang & Kwok 1993).

As far as we restrain to standard stellar evolution theory, such a shorter (or even a vanishing) PN lifetime can be obtained in three different (and to some extent mutually exclusive) ways, either

- (i) by increasing the stellar core mass so that nuclear evolution speeds up (see footnote 1),
- (ii) by delaying the Hot-PAGB phase of the stellar core (for instance, by increasing τ_{H} in equation 9) such as to let the nebula evaporate before it can be excited, or
- (iii) by fully inhibiting the AGB phase so that the PN event cannot take place, at least in a fraction of the galaxy stellar population.

Each of these different scenarios leaves a different ‘signature’ in the overall shape of the PNLF and its bright cut-off luminosity. Definitely, case (i) above is the less favoured one in our analysis, as it would predict *bluer* ellipticals to have a lower value of α , contrary to what we observe. Likely, case (ii) and (iii) better fit with an overall evolutionary scenario dominated by low-mass (old?) PAGB stars, and they could be at work at the same time (though to a different relative degree) among the PN population of early-type galaxies, as the recent *Hubble Space Telescope* (HST) observations of M 32 (Brown et al. 2000) seem to support. According to the arguments of Section 2.3.3, the core mass range $0.52 \lesssim M_{\text{core}} \lesssim 0.55 M_{\odot}$ may be the preferred one to explain the case (ii) scenario, while a more intense core mass depletion, leading to $M_{\text{core}} \lesssim 0.52 M_{\odot}$, would cause a fraction of post-HB stars to override the PN event, like in case (iii).

⁸ Note that our definition of the PN lifetime relates to the nebula visibility phase, and it is different from the kinematic age of the system, as derived from the ratio between absolute size of the main nebular shell and its expansion velocity (see, e.g. Villaver et al. 2002, for a discussion).

Table 6. The updated PN sample for local and distant early-type galaxies^a.

NGC	$\log \sigma$ (km s^{-1})	$(B - V)_o$ (mag)	Mg_2 (mag)	$(1550 - V)_o$ (mag)	$\log \alpha^b$	Ref.	Notes
205	1.61	0.82	0.071	1.19	-6.88	(1)	Star forming
221	1.90	0.88	0.198	4.50	-6.77	(1)	M32
224	2.27	0.95	0.324	3.51	-6.94	(1)	M31 (bulge only)
1316 ^c	2.38	0.87	0.265	5.0 ^d	-7.50	(2)	For A – merger
1344	2.22	0.85	0.267		-6.75	(2)	
1399	2.52	0.95	0.357	2.05	-7.30	(2)	
3031 ^c	2.23	0.82	0.295		-6.80	(1)	
3115	2.45	0.94	0.309	3.43	-6.59	(2)	
3377 ^c	2.16	0.84	0.273		-6.43	(1)	
3379	2.33	0.94	0.329	3.86	-6.77	(2)	
3384 ^c	2.20	0.91	0.296	3.9 ^d	-6.42	(1)	
4374	2.48	0.94	0.323	3.55	-6.77	(1)	
4382	2.24	0.88	0.242	4.22	-6.70	(1)	
4406	2.42	0.90	0.330	3.72	-6.89	(1)	
4472	2.49	0.95	0.331	3.42	-7.16	(1)	
4486	2.60	0.93	0.303	2.04	-7.10	(1)	
4594 ^c	2.41	0.84	0.340		-6.66	(1)	
4649	2.56	0.95	0.360	2.24	-7.22	(1)	
4697	2.25	0.89	0.320	3.41	-6.82	(2)	
5128 ^c	2.14	0.88		$\gg 5$? ^e	-6.30	(1)	Cen A – merger

References for α estimates: (1) Hui et al. (1993); (2) this paper.

^aStellar velocity dispersion $\log \sigma$, Mg_2 index and $(1550 - V)_o$ colour from Burstein et al. (1988) unless otherwise stated; reddening-corrected $(B - V)$ from the RC3 catalog (de Vaucouleurs et al. 1991).

^bFor the Hui et al. (1993) data, $\log \alpha = \log \alpha_{2.5} + 1.00$.

^c $\log \sigma$ and Mg_2 from HyperLeda Lyon.

^d $(1550 - V)$ colour estimated from the UV galaxy catalog of Rifatto et al. (1995) and RC3/HyperLeda dereddened total V magnitude. Reddening correction is according to Seaton (1979), assuming a Galaxy extinction map from Burstein & Heiles (1984).

^eConservative estimate on the basis of the upper limit to the 1540-Å galaxy flux, as reported by the NED data base.

5.1 PN core mass and M^* invariance

Within some still large theoretical uncertainties, stellar evolution models (Méndez & Soffner 1997; Marigo et al. 2004) agree on the fact that the brightest PNe are not always related to the most massive cores. Nonetheless, stars of $M_i \gtrsim 2 M_\odot$, ending up their PAGB evolution with $M_{\text{core}} \gtrsim 0.7 M_\odot$ (cf. Fig. 4), are required to generate the M^* nebulae (see e.g. fig. 10 in Marigo et al. 2004).

If our models for PN evolution are correct, then one predicts low-mass nebulae ($M_{\text{core}} \lesssim 0.65 M_\odot$) to dominate the PNLf of galaxies of different morphological type. In fact, such a claim is even stronger for ellipticals, for which very low core-mass values must be invoked on average for their old metal-rich stellar populations. Therefore, it becomes harder in these galaxies to justify the presence of relatively high-mass nebulae reaching the M^* luminosity, as the empirical invariance of the PNLf bright cut-off magnitude may imply.

A pragmatic approach to the problem has recently been pursued by Ciardullo et al. (2005), who argued on the possible presence of a blue-straggler (BS) stellar population in ellipticals, via coalescence of close binary systems. BSs are commonly observed in Galactic open clusters of all ages (e.g. Kinman 1965; Eggen & Sandage 1969) and in some globulars, too (e.g. Buonanno et al. 1994), and these objects may in principle reach up to twice the TO mass, that is $\sim 2 M_\odot$, even in old stellar systems. While ensuring a convenient fraction of M^* nebulae and account for the observed M^* invariance, this scenario still leaves, however, a few open question, which we address below.

5.2 Diagnostic planes

To evaluate the impact of the different AGB and PAGB evolutionary pictures in elliptical galaxies, it may be useful to investigate the correlations of α with other observed quantities for the galaxy sample of Table 6, as displayed in Figs 11–13.

The plot of the Lick Mg_2 index (Faber et al. 1985) in Fig. 11 is of special interest, in this regard, because it is the least affected by reddening. Here, the α correlation with galaxy colour is more cleanly replicated, suggesting that metallicity, rather than age, is the relevant parameter that affects the observed PN rate per unit galaxy luminosity. With the exception of NGC 1316 (Fornax A), that we shall discuss in some details, the plot shows that a lower number of PNe per unit galaxy luminosity is produced in metal-rich ellipticals.

As chemical and dynamical properties are tightly correlated in early-type galaxies (Faber & Jackson 1976; Terlevich et al. 1981; Burstein et al. 1984), one may expect some correlation of α with the galaxy internal velocity dispersion too (that is, roughly, with the galaxy total mass). This is shown in Fig. 12. Among others, the good fit of the M 31 bulge to the overall correlation for early-type systems in Figs 11 and 12 could be considered as an additional piece of evidence of the similarity between the stellar populations of spiral bulges and ellipticals (Jablonka, Martin & Arimoto 1996).

The general picture of PN evolution, sketched in Section 2.3, especially reflects in the distinctive properties of the early-type galaxy population in the UV spectral range. In particular, the two relevant post-HB evolutionary paths, that lead stars either to a full AGB

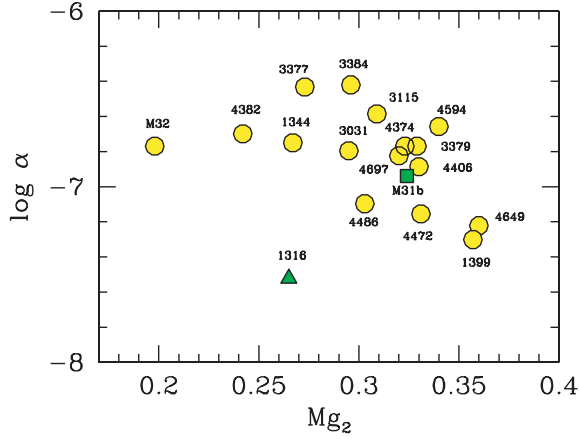


Figure 11. The observed distribution of the elliptical galaxy sample of Table 6 (plus M 32 and the bulge of M 31, as labelled on the plot) versus Lick spectrophotometric index Mg_2 . Note the relative lack of PNe (per unit galaxy luminosity) in more metal rich ellipticals. The relevant case of the merger galaxy NGC 1316 is singled out, while the active star-forming elliptical NGC 205 is out of range with $Mg_2 \lesssim 0.1$ and not shown. See text for a discussion.

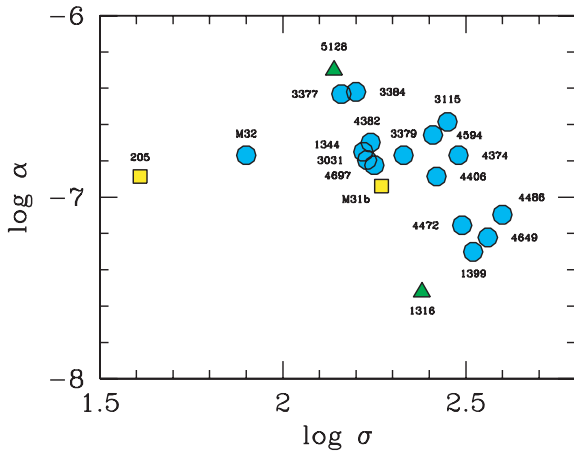


Figure 12. Same as Fig. 11, but for the galaxy velocity dispersion σ in km s^{-1} . It is evident a lower value of α in high- σ (roughly more massive) galaxies. See text for further details.

completion or straight to the high-temperature white dwarf cooling sequence have different impact on the galaxy spectral energy distribution (SED) at short wavelength compared to the optical luminosity. To explore this important feature, in Fig. 13, we plot the $\log \alpha$ values versus the UV colour $(1550 - V) = -2.5 \log [f(1550 \text{ \AA})/f(V)]$, as first defined by Burstein et al. (1988), where the galaxy SED is measured at 1550 \AA and in the Johnson V band. The $(1550 - V)$ colour, from *IUE (International Ultraviolet Explorer)* observations and corrected for Galaxy extinction, was provided by Burstein et al. (1988) for a fraction of galaxies in Table 6.⁹

⁹ The $(1550 - V)$ colour for NGC 1316 and NGC 3384 has also been added to Table 6, as obtained from the Rifatto, Longo & Capaccioli (1995) UV catalog. These entries, however, are reported with a larger error, as the galaxy flux at 1550 \AA derives from a crude extrapolation of the reported magnitudes at 1650 and 2500 \AA .

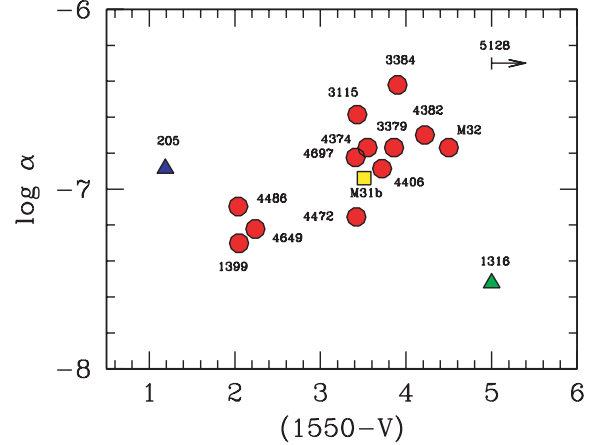


Figure 13. The luminosity-specific PN number versus UV colour $(1550 - V)$, as originally defined by Burstein et al. (1988), for the elliptical galaxy sample of Table 6 (plus the Andromeda satellites and the bulge of M 31). Some relevant cases, like NGC 205 (star forming), NGC 1316 and NGC 5128 (merger ellipticals) are singled out on the plot. Note the tight relationship between ‘quiescent’ ellipticals and α , with UV-bright galaxies to be also PN-poor. See text for a full discussion of this important effect.

Fig. 13 shows a tight correlation between the value of α and the UV emission, with massive UV-enhanced ellipticals, like NGC 4649 and NGC 4486 in Virgo, or NGC 1399 in Fornax that are also much poorer in PNe. To a finer analysis of the plot, one can even notice an apparent gap (marginally evident also in Fig. 12) between these three giant ellipticals and the bulk of more ‘normal’ galaxies (including the bulge of M 31).

One may speculate that the bulk of the PN population in ‘normal’ ellipticals evolves according to the case (ii) scenario; a substantial fraction of stars, in these galaxies, would therefore complete its AGB evolution leading to low-mass PNe, with $M_{\text{core}} \leq 0.55 M_{\odot}$. The intervening increase of the AGB \Rightarrow Hot-PAGB transition time in this mass range, would eventually shorten the nebula lifetime and reduce τ_{PN} from $\sim 30\,000$ to $\sim 10\,000$ yr or less, as for the stellar population in the M 31 bulge (see Fig. 10). If the mean PAGB core mass is further decreased in more massive galaxies, perhaps as a consequence of a stronger mass loss, then one may expect an increasing fraction of HB stars to feed the *AGB-manqué* evolutionary channel and fail to produce PNe, as in case (iii) scenario. This would imply an even lower value of α and a strongly enhanced galaxy UV emission, as observed in NGC 4649, NGC 4486 and NGC 1399 in Fig. 13.

In this framework, the envisaged role of the BS stellar component could be assessed on the basis of the Xin & Deng (2005) analysis of a sample of old ($t \geq 5$ Gyr) Galactic open clusters. A sizable presence of BSs is found to severely affect cluster colours, by shifting the integrated $B - V$ over ~ 0.2 mag to the blue (see Fig. 14). When applied to ellipticals, this argument could place a quite tight constraint to the overall BS luminosity contribution, and the size of the induced PN progeny, in order to avoid unrealistically bluer galaxy colours. For example, if we take the case of cluster M 67 (the Praesepe) as a reference, BSs are found to supply ~ 50 per cent of the total B luminosity (Deng et al. 1999), causing a $\Delta(B - V) = -0.15$ mag shift to the integrated cluster colour (Xin & Deng 2005). Converting these values to bolometric luminosities (e.g. by relying on our discussion in Section 3.1.1), this implies that BS contribution must be *well below* ~ 10 per cent of the total galaxy luminosity if

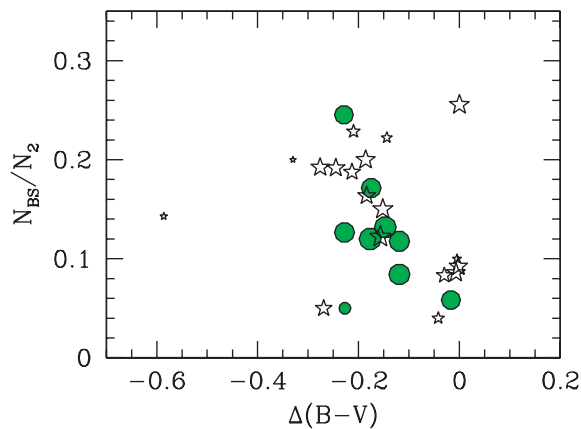


Figure 14. The blue shift of the integrated $B - V$ colour of old open clusters in the Galaxy caused by the BS stellar population, from Xin & Deng (2005). The BS component (N_{BS}) is normalized in terms of its ratio to the number of MS stars down to 2 mag below the TO luminosity (N_2). Solid dots are for the oldest ($t \geq 5$ Gyr) clusters, while star markers include clusters with $1 \leq t < 5$ Gyr. Symbol size is proportional to cluster statistical richness.

we wish to avoid any measurable effect on the integrated optical colours of ellipticals.

In addition, if M^* PNe in ellipticals really stem from BS evolution, then one consequence is that the value of α for these galaxies, as extrapolated from the observation of the very brightest nebulae alone, could sensibly overestimate the population of ‘standard’ (i.e. single-star) PNe of lower core mass. According to equation (21), this would imply an even shorter mean lifetime for single-star nebulae, thus enforcing the importance of the cases (ii) and (iii) evolutionary channels. If two PN subpopulations of bright (coalesced) PNe and fainter nebulae generated from standard evolution of low-mass stars really co-exist in early-type galaxies, then one might wonder whether they also display any distinctive dynamical signature, as the recent case of NGC 4697 (Sambhus, Gerhard & Mendez 2006) seem to suggest.

To complete the discussion of Fig. 13, we now focus on two major outliers in the plot, namely NGC 205 and NGC 1316. The first case can easily be assessed as this M 31 dwarf satellite is known to undergo active star formation (e.g. Bica, Alloin & Schmidt 1990; Lee 1996) and its strong UV emission (as well as its exceedingly low Mg_2 index, see Table 6) is in fact the result of young (a few 10^8 yr) MS stars. More special attention, instead, must be paid to the case of NGC 1316 (Fornax A).

5.3 Galaxy environment and PN evolution: the case of NGC 1316 and Cen A

Together with NGC 5128 (Cen A), NGC 1316 is known as one of the best established examples of ‘mergers’ among early-type systems (Schweizer 1983; Goudfrooij et al. 2001). The study of these two galaxies may therefore lead to a preliminary assessment of the influence of ‘active’ galaxy environments on the PN population.

The location of both objects in the $\log \sigma$ plot of Fig. 12 places them at the extreme (both highest and lowest) values of α ; furthermore, one must also report the peculiar location of NGC 1316 in the Mg_2 plot (Fig. 11), which shows a severe PN deficiency when comparing for instance with NGC 4382, of similar mass and metal-

licity.¹⁰ Regarding the UV properties of these ‘merger templates’, the upper limit to the 1540-Å flux for NGC 5128, as reported by the NED data base, suggests a presumably very ‘red’ UV colour for this galaxy, such as $(1550 - V)_o \gg 5$, in line with the observations of NGC 1316.

Definitely, in spite of similar observed spectrophotometric properties (i.e. $\log \sigma$, $(B - V)_o$ and, likely, the $(1550 - V)_o$ colour, cf. Table 6), it remains difficult to understand the role of galaxy merging mechanisms that led, for Cen A and For A, to such a dramatically different behaviour in terms of PN population.

6 DISCUSSION AND CONCLUSIONS

Wide-field CCD detectors, and accurate selection criteria based on $H\alpha$ and [O III] narrow-band photometry, allow a systematic survey of the PN population both in the Milky Way and in external galaxies. Deep observations now explore the PNLF several magnitudes below the bright cut-off, as recently achieved in the SMC (Jacoby 2006). The corresponding developments in the theoretical modelling help in clarifying the main physical mechanisms that constrain the nebular properties, especially those related to shell dynamics (e.g. Villaver et al. 2002; Perinotto et al. 2004a) and chemical composition (Liu et al. 2004; Perinotto, Morbidelli & Scatarzi 2004b), although a clear understanding of the the PNLF at bright and low magnitudes is still to come.

One open question deals with the empirical evidence for a nearly constant absolute magnitude of the PNLF bright cut-off (M^*), which makes bright PNe effective standard candles for the intermediate cosmic distance scale ($\lesssim 100$ Mpc; Jacoby 1989; Ciardullo et al. 2002a). This feature is not explained by the theoretical models, which predict M^* to be a function of age, metallicity and other distinctive properties of the parent stellar population (Marigo et al. 2004). In particular, this problem is stronger for elliptical galaxies, where a lower TO mass for their stellar populations may hardly reconcile with the required presence of $\sim 2 M_\odot$ stellar progenitors for the M^* nebulae (Marigo et al. 2004; Ciardullo et al. 2005).

The PNLF faint-end tail is also subject to a substantial uncertainty, with observations showing a decrease in the number of PN at about 6-mag fainter than M^* (Jacoby & De Marco 2002), and theory which predicts a distribution reaching magnitudes as faint as 8-mag below the PNLF bright cut-off. We have discussed in Section 4.1 that our limited knowledge of the PNLF faint end reflects in a factor of 2 uncertainty on the estimated total number of nebulae for a given stellar system. The errors become larger for the most distant galaxies, external to the LG. In most cases, the PNLF is only sampled in its brightest magnitude bin, and the observed PNe number must be multiplied by a factor of 20–40 (see Table 3) to provide an estimate for the whole PN population.

Despite these large uncertainties, the study of the luminosity-specific PN number (the so-called ‘ α ’ parameter in our discussion) in external galaxies has allowed us to tackle the properties of the PN population in different environments, from dense bulge-dominated galaxies to very low density stellar populations such as those of the intracluster diffuse stellar component (Feldmeier et al. 2004; Aguerri et al. 2005). From the theory presented in Section 2 and 5, there is a close *liason* between the value of α and the PN visibility lifetime: as the specific evolutionary flux, \mathcal{B} , in equation (3) is nearly

¹⁰ Unfortunately, the lack of Mg_2 data for NGC 5128 prevents a similar comparison for this galaxy.

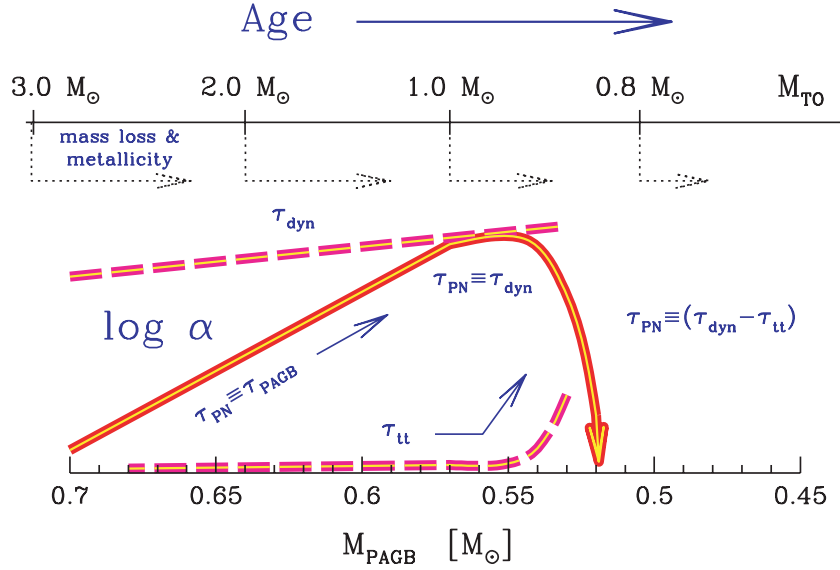


Figure 15. A representation of the envisaged PN evolution versus core mass of PAGB stars. The effect of different parameters, like metallicity, mass loss and age is outlined. In particular three evolutionary regimes are singled out, with PN visibility lifetime τ_{PN} (and correspondingly α) constrained respectively by the nuclear time-scale (τ_{PAGB}), shell dynamics (τ_{dyn}) and transition time (τ_{tt}). PN visibility drastically reduces for $M_{\text{core}} \lesssim 0.55 M_{\odot}$ until reaching a critical limit for PN formation about $M_{\text{core}} \simeq 0.52 M_{\odot}$. See text for full discussion.

constant, then

$$\tau_{\text{PN}} \approx 30\,000 (\alpha/5.4 \cdot 10^{-7}) \text{ yr.} \quad (22)$$

Depending on the stellar core mass at the beginning of the AGB phase, the value of τ_{PN} must be compared with three relevant time-scales that determine the PN evolution. As sketched in Fig. 15, they are the PAGB core lifetime (τ_{PAGB}), the dynamical time-scale for the nebula evaporation (τ_{dyn}) and the transition time for the stellar core to leave the AGB and reach the high-temperature regime required to trigger the nebula [O III] emission (τ_{tt}). Along the SSP evolution, mass loss eventually settles the absolute clock that links the τ_{PN} evolution with the SSP age (see Section 2.4).

As far as core evolution provides the leading time-scale for the PN visibility, standard mass-loss theory *à la* Reimers (1975) predicts that τ_{PN} (and correspondingly α) *should increase with SSP age*.¹¹ More generally, one would expect this to be the case of late-type galaxies, where star formation is on-going and a consistent fraction of high-mass stars is younger than a few Gyr (cf. Fig. 6). As the fraction of young stars is higher in irregulars than in elliptical galaxies, and the integrated $B - V$ colour becomes bluer along the $E \rightarrow \text{Im}$ Hubble morphological sequence, then *one may conclude that lower values of α are expected in bluer galaxies*.

However, observationally this does not occur for the LG galaxy population, as shown in Fig. 10. In fact, while the suggested theoretical range for α in the $\eta = 0.3$ models matches the observations *on average*, the latter points to a constant behaviour with galaxy morphological type, with a typical rate between 1 and 6 PNe per $10^7 L_{\odot}$. From these observations, the inferred PN lifetime in LG spirals and irregulars should exceed 10 000 yr, a value that requires the presence of a substantial fraction of stars with $M_{\text{core}} \lesssim 0.65 M_{\odot}$

(cf. Fig. 5) even in those galaxies with the most active star formation activity.

The relatively low final mass and the tight mass range required by the ‘dying’ stars in external galaxies find independent confirmation in the Milky Way, as also indicated by the observational evidence of the IFMR for local open clusters by W00. We have shown in Section 4.1 that population synthesis models using this empirical IFMR produce a better fit (both in absolute value and relative trend with galaxy morphological type) for the correct value of PN density per unit galaxy luminosity in the LG galaxies, along the whole Hubble morphological sequence (see Fig. 10). This result indicates that the dynamical evolution plays a central role in setting the overall PN observed properties as for low core-mass stars, the dynamical rather than nuclear time-scale is the real driving parameter to constrain PN visibility (see Fig. 15). As a consequence, one may state that, *rather than probing any real mass distribution of PAGB stars, the PNLF basically tracks the time evolution of the expanding shell around stellar nuclei of nearly fixed mass* (Henize & Westerlund 1963).

Within this picture, one problem is related with the PN evolution in (giant) elliptical galaxies. Here, the empirical evidence for a constant PNLF bright cut-off magnitude would require a sizable component of relatively high-mass stars, well above the TO mass of $\sim 1 M_{\odot}$ expected for these old stellar systems. Following Ciardullo et al. (2005), BS stars originating from coalesced close binary systems according to a classical evolutionary scheme (McCrea 1964), may possibly overcome the dilemma. However, if ellipticals do indeed host a BS population in a fraction similar to what we detect in old Galactic open clusters, then galaxies should appear roughly 0.2-mag bluer than observed, in $B - V$ (see Fig. 14). As a consequence, from our arguments in Section 5.2, one is led to conclude that, in any case, BSs cannot provide much more than a few percent of galaxy bolometric luminosity and *PNe coming from the BS progeny must be confined to the very brightest bin of the PNLF, thus representing a marginal fraction of the global PN population*.

The relative lack of massive stars in early-type galaxies, and a high (supersolar?) metallicity possibly easing a stronger mass loss

¹¹ For a characteristic value of the mass-loss parameter η , we have from IR83 that the final mass of PN nuclei roughly scales as $M_{\text{PAGB}} \propto \eta^{-0.35} t^{-0.29}$, recalling that, to a first approximation, $t \propto M_{\text{TO}}^{-3.5}$ (Buzzoni 2002). According to footnote 1, this eventually leads to $\tau_{\text{PAGB}} \propto \eta^{2.2} t^{1.8}$.

in these galaxies, might actually lead to a larger component of blue HB stars, eventually evolving into low-mass PNe. In Section 2.3, we have seen that for the low-mass cores ($M_{\text{core}} \lesssim 0.55 M_{\odot}$), the increase in the transition time τ_{tr} reduces effectively the visibility time-scale of the nebula (see, again Fig. 15), thus decreasing the value of α . This trend is expected to depend on galaxy colour (or metallicity, as shown by the Mg_2 distribution of Fig. 11) with a lower PN density per unit galaxy luminosity for the redder ellipticals.

Furthermore, for the stellar component with $M_{\text{core}} \lesssim 0.52 M_{\odot}$, both HB and post-HB evolution occur at high temperature ($T_{\text{eff}} \gg 10^4$ K) thus skipping the PN phase entirely (Castellani & Tornambé 1991; Dorman et al. 1993; Blöcker 1995). For these stars, the *AGB-manqué* evolution can effectively transfer some fraction of the PAGB energy budget to the hot HB tail and affect the integrated galaxy SED. As a consequence, one may expect that the most UV-enhanced ellipticals display also the lowest values of α . We have shown in Section 5 that such a tight correlation is observed for elliptical galaxies in the Virgo cluster and other groups (see Fig. 13). Recent *HST* observations of the resolved stellar population of M 32 and the bulge of M 31 (Brown et al. 1998, 2000) further support this proposed scenario.

The presence in our sample of two merger galaxies (Fornax A and Cen A) may provide the opportunity to study the effect of galaxy interactions on the PN population. Based on the available data however, no firm conclusions can be drawn, although one has to remark that these two galaxies stand out as those with the most extreme (both highest and lowest) values of α in our sample. Perhaps such a huge variation in the galaxy PN population may be related to the disruptive effect of the intergalactic ram pressure, as recently considered by Villaver, García-Segura & Manchado (2003) and Villaver & Stanghellini (2005).

ACKNOWLEDGMENTS

We would like to thank Robin Ciardullo, the referee of this paper, for enlightening comments on the role of blue stragglers in PN evolution of elliptical galaxies. Giuseppe Bono, Ortwin Gerhard, Laura Greggio, Detlef Schönberner and Letizia Stanghellini are also acknowledged for useful discussions and suggestions on earlier drafts of this work. This project received financial support by INAF, under grants PRIN/02 (PI: MA) and PRIN/05 (PI: AB), and the Swiss National Foundation. Our analysis has made extensive use of different on-line extragalactic data bases, namely the NASA/IPAC Extragalactic Database (NED), operated by JPL/CIT under contract with NASA, the Hyper-Linked Extragalactic Databases and Archives (HyperLeda) based at the Lyon University, and the VizieR catalog service of the Centre de Données astronomiques de Strasbourg.

REFERENCES

Aguerrí J. A. L., Gerhard O. E., Arnaboldi M., Napolitano N. R., Castro-Rodríguez N., Freeman K. C., 2005, *AJ*, 129, 2585
 Allen C., Kinman T., 2004, *Rev. Mex. Astron. Astrofis. Ser. Conf.*, 21, 121
 Alloin D., Cruz-González C., Peimbert M., 1976, *ApJ*, 205, 74
 Arnaboldi M., 2004, in Duc P.-A., Braine J., Brinks E., eds, *IAU Symp. 217, Recycling Intergalactic and Interstellar Matter.*, Astron. Soc. Pac., San Francisco, p. 54
 Arnaboldi M., Freeman K. C., Hui X., Capaccioli M., Ford H., 1994, *The Messenger*, 76, 40
 Arnaboldi M., Freeman K. C., Gerhard O., Matthias M., Kudritzki R. P., Méndez R. H., Capaccioli M., Ford H., 1998, *ApJ*, 507, 759
 Arnaboldi M. et al., 2003, *AJ*, 125, 514

Arnaboldi M., Gerhard O., Aguerrí J. A. L., Freeman K. C., Napolitano N. R., Okamura S., Yasuda N., 2004, *ApJ*, 614, 33
 Baade W., 1955, *AJ*, 60, 151
 Bica E., Alloin D., Schmidt A. A., 1990, *A&A*, 228, 23
 Blaauw A., 1961, *Bull. Astron. Inst. Netherlands*, 15, 265
 Blöcker T., 1995, *A&A*, 299, 753
 Boissier S., Prantzos N., 1999, *MNRAS*, 307, 857
 Brown T. M., Ferguson H. C., Stanford S. A., Deharveng J.-M., 1998, *ApJ*, 504, 113
 Brown T. M., Bowers C. W., Kimble R. A., Sweigart A. V., Ferguson H. C., 2000, *ApJ*, 532, 308
 Buonanno R., Corsi C. E., Buzzoni A., Cacciari C., Ferraro F. R., Fusi Pecci F., 1994, *A&A*, 290, 69
 Burstein D., Heiles C., 1984, *ApJS*, 54, 33
 Burstein D., Faber S. M., Gaskell C. M., Krumm N., 1984, *ApJ*, 287, 586
 Burstein D., Bertola F., Buson L. M., Faber S. M., Lauer T. R., 1988, *ApJ*, 328, 440
 Buzzoni A., 1989, *ApJS*, 71, 817 (B89)
 Buzzoni A., 1995, *ApJS*, 98, 69
 Buzzoni A., 1998, in Zanzu T., Testa V., Bellazzini M., eds, *Evolving Evolution. Oss. di Cagliari, Cagliari*, p. 13
 Buzzoni A., 2002, *AJ*, 123, 1188
 Buzzoni A., 2005, *MNRAS*, 361, 725
 Caldwell N., 1995, in Buzzoni A., Renzini A., Serrano A., eds, *Fresh Views of Elliptical Galaxies.* Astron. Soc. Pac., San Francisco, p. 93
 Castellani M., Tornambé A., 1991, *ApJ*, 381, 393
 Castellani M., Limongi M., Tornambé A., 1992, *ApJ*, 389, 227
 Castellani M., Limongi M., Tornambé A., 1995, *ApJ*, 450, 275
 Castellani V., Iannicola G., Bono G., Zoccali M., Cassisi S., Buonanno R., 2006, *A&A*, 446, 569
 Cellone S. A., Buzzoni A., 2005, *MNRAS*, 356, 41
 Ciardullo R., Jacoby G. H., Ford H. C., Neill J. D., 1989, *ApJ*, 339, 53
 Ciardullo R., Feldmeier J. J., Jacoby G. H., Kuzio de Naray R., Laychak M. B., Durrell P. R., 2002a, *ApJ*, 577, 31
 Ciardullo R., Feldmeier J. J., Krelove K., Jacoby G. H., Gronwall C., 2002b, *ApJ*, 566, 784
 Ciardullo R., Durrell P. R., Laychak M. B., Herrmann K. A., Moody K., Jacoby G. H., Feldmeier J. J., 2004, *ApJ*, 614, 167
 Ciardullo R., Sigurdsson S., Feldmeier J. J., Jacoby G. H., 2005, *ApJ*, 629, 499
 Claver C. F., Liebert J., Bergeron P., Koester D., 2001, *ApJ*, 563, 987
 Corradi R. L. M., Magrini L., 2006, in Walsh J. R., Stanghellini L., Douglas N., eds, *ESO Astrophys. Symp., Planetary Nebulae Beyond the Milky Way.* Springer-Verlag, Heidelberg, in press
 Corradi R. L. M. et al., 2005, *A&A*, 431, 555
 D’Cruz N. L., Dorman B., Rood R. T., O’Connell R. W., 1996, *ApJ*, 466, 359
 Deng L., Chen R., Liu X. S., Chen J. S., 1999, *ApJ*, 524, 824
 de Vaucouleurs G., de Vaucouleurs A., Corwin H. G., Jr, Buta R. J., Paturel G., Fouque P., 1991, *Third Reference Catalog of Bright Galaxies.* Springer-Verlag, Heidelberg
 Dominguez I., Chieffi A., Limongi M., Straniero O., 1999, *ApJ*, 524, 226
 Dopita M. A., Jacoby G. H., Vassiliadis E., 1992, *ApJ*, 389, 27
 Dorman B., Rood R. T., O’Connell R. W., 1993, *ApJ*, 419, 596
 Douglas N. G. et al., 2002, *PASP*, 114, 1234
 Eggen O. J., Sandage A. R., 1969, *ApJ*, 158, 669
 Faber S. M., Jackson R. E., 1976, *ApJ*, 204, 668
 Faber S. M., Friel E. D., Burstein D., Gaskell C. M., 1985, *ApJS*, 57, 711
 Feldmeier J. J., Ciardullo R., Jacoby G. H., Durrell P. R., 2003, *ApJS*, 145, 65
 Feldmeier J. J., Ciardullo R., Jacoby G. H., Durrell P. R., 2004, *ApJ*, 615, 196
 Fusi Pecci F., Renzini A., 1976, *A&A*, 46, 447
 Gerhard O., Arnaboldi M., Freeman K. C., Kashikawa N., Okamura S., Yasuda N., 2005, *ApJ*, 621, 93
 Gingold R. A., 1974, *ApJ*, 193, 177
 Girardi L., Bressan A., Bertelli G., Chiosi C., 2000, *A&AS*, 141, 371
 Górny S. K., Tylenda R., Szczerba R., 1994, *A&A*, 284, 949

- Goudfrooij P., Mack J., Kissler-Patig M., Meylan G., Minniti D., 2001, *MNRAS*, 322, 643
- Greggio L., Renzini A., 1990, *ApJ*, 364, 35
- Grevesse N., Noels A., Sauval A. J., 1996, in Holt S. S., Sonneborn G., eds, *ASP Conf. Ser., Vol. 99, Cosmic Abundances. Astron. Soc. Pac., San Francisco*, p. 117
- Henize K. G., Westerlund B. E., 1963, *ApJ*, 137, 747
- Hui X., Ford H. C., Ciardullo R., Jacoby G. H., 1993, *ApJ*, 414, 463
- Hunter D. A., Gallagher J. S., III, 1985, *ApJS*, 58, 533
- Iben I., Jr, Renzini A., 1983, *ARA&A*, 21, 271 (IR83)
- Jablonka P., Martin P., Arimoto N., 1996, *AJ*, 112, 1415
- Jacoby G., 1980, *ApJ*, 42, 1
- Jacoby G., 1989, *ApJ*, 339, 39
- Jacoby G., 2006, in Walsh J. R., Stanghellini L., Douglas N., eds, *ESO Astrophys. Symp., Planetary Nebulae Beyond the Milky Way. Springer-Verlag, Heidelberg*, in press
- Jacoby G., De Marco O., 2002, *AJ*, 123, 269
- Kalirai J. S., Richer H. B., Reitzel D., Hansen B. M. S., Rich R. M., Fahlman G. G., Gibson B. K., von Hippel T., 2005, *ApJ*, 618, L123
- Karachentsev I. D., 2005, *AJ*, 129, 178
- Keenan F. P., Dufton P. L., 1983, *MNRAS*, 205, 435
- Kinman T. D., 1965, *ApJ*, 142, 655
- Kwok S., 1994, *PASP*, 106, 344
- Lee M. G., 1996, *AJ*, 112, 1438
- Liu Y., Liu X.-W., Barlow M. J., Luo S.-G., 2004, *MNRAS*, 353, 1251
- Magrini L., Corradi R. L. M., Mampaso A., Perinotto M., 2000, *A&A*, 355, 713
- Marigo P., Girardi L., Groenewegen M. A. T., Weiss A., 2001, *A&A*, 378, 958
- Marigo P., Girardi L., Weiss A., Groenewegen M., Chiosi C., 2004, *A&A*, 423, 995
- Martin N. F., Ibata R. A., Bellazzini M., Irwin M. J., Lewis G. F., Dehnen W., 2004, *MNRAS*, 348, 12
- McCrea W. H., 1964, *MNRAS*, 128, 335
- Méndez R. H., Soffner T., 1997, *A&A*, 321, 898
- Méndez R., Kudritzki R. P., Ciardullo R., Jacoby G. H., 1993, *A&A* 275, 534
- Méndez R., Riffeser A., Kudritzki R. P., Matthias M., Freeman K. C., Arnaboldi M., Capaccioli M., Gerhard O., 2001, *ApJ*, 563, 135
- Merrett H. R. et al., 2003, *MNRAS*, 346, L62
- Mihos J. C., Harding P., Feldmeier J., Morrison H., 2005, *ApJ*, 631, 41
- Paczyński B., 1970, *Acta Astron.*, 20, 47
- Paczyński B., 1971, *Acta Astron.*, 21, 417
- Peimbert M., 1990, *Rev. Mex. Astron. Astrofis.*, 20, 119
- Peng E. W., Ford H. C., Freeman K. C., 2004, *ApJ*, 602, 685
- Perinotto M., Schönberner D., Steffen M., Calonaci C., 2004a, *A&A*, 414, 993
- Perinotto M., Morbidelli L., Scatarzi A., 2004b, *MNRAS*, 349, 793
- Phillips J. P., 1989, in Torres-Peimbert S., ed., *Planetary Nebulae. Kluwer, Dordrecht*, p. 425
- Reimers D., 1975, *Mem. Soc. R. Sci. Liège*, 6th Ser., 8, 87
- Renzini A., 1981, in Iben I., Jr, Renzini A., eds, *Physical Processes in Red Giants. Reidel, Dordrecht*, p. 431
- Renzini A., Buzzoni A., 1986, in Chiosi C., Renzini A., eds, *Spectral Evolution of Galaxies. Reidel, Dordrecht*, p. 195 (RB86)
- Rifatto A., Longo G., Capaccioli M., 1995, *A&AS*, 114, 527
- Robin A. C., Reylé C., Derrière S., Picaut S., 2003, *A&A*, 409, 523
- Romanowsky A. J., Douglas N. G., Arnaboldi M., Kuijken K., Merrifield M. R., Napolitano N. R., Capaccioli M., Freeman K. C., 2003, *Sci*, 301, 1696
- Sambhus N., Gerhard O., Méndez R. H., 2006, *AJ*, 131, 837
- Schönberner D., 1981, *A&A*, 103, 119
- Schönberner D., 1983, *ApJ*, 272, 708
- Schweizer F., 1983, in Athanassoula E., ed., *IAU Symp., 100, Internal Kinematics and Dynamics of Galaxies. Reidel, Dordrecht*, p. 319
- Seaton M. J., 1979, *MNRAS*, 187, 73p
- Stanghellini L., 1995, *ApJ*, 452, 515
- Stanghellini L., Renzini A., 2000, *ApJ*, 542, 308
- Teodorescu A. M., Méndez R. H., Saglia R. P., Riffeser A., Kudritzki R. P., Gerhard O. E., Kleya J., 2006, *ApJ*, 635, 290
- Terlevich R., Davies R. L., Faber S. M., Burstein D., 1981, *MNRAS*, 196, 381
- Uson J. M., Boughn S. P., Kuhn J. R., 1991, *ApJ*, 369, 46
- Vassiliadis E., Wood P. R., 1994, *ApJS*, 92, 125
- Villaver E., Stanghellini L., 2005, *ApJ*, 632, 854
- Villaver E., Manchado A., García-Segura G., 2002, *ApJ*, 581, 1204
- Villaver E., García-Segura G., Manchado A., 2003, *ApJ*, 585, 49
- Wagenhuber J., Weiss A., 1994, *A&A*, 286, 121
- Weidemann V., 1987, *A&A*, 188, 74
- Weidemann V., 2000, *A&A*, 363, 647 (W00)
- Weidemann V., Koester D., 1983, *A&A*, 121, 77
- Xin Y., Deng L., 2005, *ApJ*, 619, 824
- Yi S., Demarque P., Oemler A. J., 1998, *ApJ*, 492, 480
- Zhang C. Y., Kwok S., 1993, *ApJS*, 88, 137

This paper has been typeset from a $\text{\TeX}/\text{\LaTeX}$ file prepared by the author.